

Theoretical Investigation of Complex Potentials for Atomic Collisions.

I. Numerical Solution of Model (H^- , H) Collisions*

Junya Mizuno and Joseph C. Y. Chen

Department of Physics and Institute for Pure and Applied Physical Sciences, University of California, San Diego, La Jolla, California 92037

(Received 4 June 1969)

A set of coupled equations for rearrangement collisions involving processes such as scattering, electron transfer ($A^- + B \rightarrow A + B^-$), collisional detachment ($A^- + B \rightarrow A + B + e$), and associative detachment ($A^- + B \rightarrow AB + e$) is solved numerically for the (H^- , H) collision system at low energies. In this calculation, the interaction potential between the ground states of H and H^- is approximated by a set of local complex potentials. The energy dependence and scattering-angle dependence of the electron-detachment and electron-transfer probabilities, and of differential cross sections for scattering, electron transfer, and detachment processes, are calculated. A detailed analysis of the interference structures in the various differential cross sections is made for the diffraction and multipath scatterings, and for the gerade-ungerade and nuclear symmetry interferences. The effect of damping due to the imaginary parts of the complex potentials and the effect of isotope substitutions are investigated. To examine the sensitivity of the calculated results to the potentials adopted, the calculations are carried out for several sets of such complex potentials. Important differences, which may provide useful information for further investigations, are found for different sets of potentials.

I. INTRODUCTION

It is now well recognized that the collisional processes resulting from the collision of negative ions with atoms and molecules are strongly coupled with the electron-detachment channels.¹⁻⁶ This coupling may persist for extremely slow collisions if the associative-detachment channel is exoergic (exothermic). Consequently, the collision of negative ions with atoms and molecules, even at energies below the electron-detachment potential, is a multichannel rearrangement problem with all its complexities. Formally, the coupling with the electron-detachment channels may be accounted for in the other channels by making the interaction between the ion and the atom (or molecule) nonlocal, energy-dependent, and complex. This well-known formal procedure⁷ turns out to be very fruitful for the present problem, because the nonlocal energy-dependent complex potential may, when the large mass disparity between the electron and the nuclei is utilized, be approximated by a set of local energy-independent complex potentials.

For the (H^- , H) collision system, the interaction potential between H^- and H when both H^- and H are in their ground states may be approximated by two sets of local complex potentials corresponding to the $^2\Sigma_u^+$ and $^2\Sigma_g^+$ H_2 adiabatic compound states. Such sets of local complex potentials for the interaction between ground states of H and H^- have been calculated by Bardsley, Herzenberg, and Mandl,⁸ and deduced semi-empirically by Chen and Peacher.⁹ The real

parts of these sets of potentials have also been calculated by Eliezer, Taylor, and Williams.¹⁰ The purpose of the present work is to utilize these potentials for the investigation of the collisional dynamics of the (H^- , H) system. In this paper, we will confine our interest to the very low-energy collisions by solving the set of appropriate coupled equations numerically.¹¹ This is an energy region that, at present, is not easily accessible for accurate experimental investigation. It is therefore of interest to obtain some theoretical predictions.

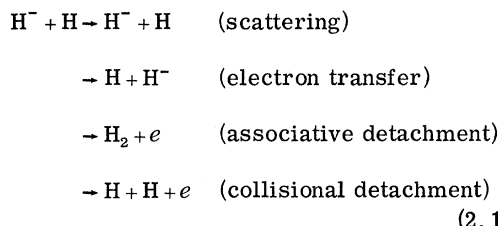
A brief review of the formulation of the coupled equations for multichannel rearrangement collision is given in Sec. II for the (H^- , H) collision system. The set of coupled equations is then simplified and expressed in terms of local complex potentials in Sec. III in a form suitable for numerical solutions. The available complex potentials are collected, compared, and then adopted for the calculations. The results and their interpretation are presented in Sec. IV, together with remarks concerning the interaction potential between the ground states of H^- and H.

II. MULTICHANNEL REARRANGEMENT COLLISIONS

The formal theory of rearrangement collisions is well documented in the book by Goldberger and Watson.¹² For computational purposes, it is often desirable to describe the collisions in the form of a set of coupled equations.¹³ Such a set of coupled equations for rearrangement collisions may be obtained in the projection-operator tech-

niques first developed by Feshbach.¹⁴ We now adopt this technique for the treatment of the (H^- , H) collision system.

We consider for the collision system the case where both H^- and H are in their ground states before the collision, and where four reaction paths



are energetically accessible after the collision. Following Feshbach,¹⁴ we may construct a projection operator P which projects onto all the open channels associated with the four reaction paths. In terms of this projection operator P , the Schrödinger equation

$$(E - H)\Upsilon = 0 \quad (2.2)$$

for the (H^- , H) collision system may be rewritten¹⁴

$$(E - \mathcal{K}_P)P\Upsilon = 0, \quad (2.3)$$

$$\text{with } \mathcal{K}_P = P \left\{ H + HQ \frac{1}{E - QHQ} QH \right\} P, \quad (2.4)$$

$$Q = 1 - P, \quad (2.5)$$

where H and Υ are the total Hamiltonian and collisional wave function of the system, respectively.

The projection operator P which projects onto the scattering, electron-transfer, and electron-detachment channels [see Eq. (2.1)] can be decomposed into projectors p_1 , p_2 , and p_3 , which project, respectively, onto each of three sets of channels.¹⁵ We have asymptotically for the scattering and electron-transfer channels

$$p_1 \Upsilon \rightarrow \mathcal{A} \varphi(\vec{r}_{1a}, \vec{r}_{2a}) \psi(\vec{r}_{3b}) \left\{ e^{i\vec{k} \cdot \vec{q}_1} + f_s(\hat{k}, \hat{q}_1) \frac{e^{ikq_1}}{q_1} \right\}, \quad (2.6)$$

as $q_1 \rightarrow \infty$,

$$p_2 \Upsilon \rightarrow \mathcal{A} \varphi(\vec{r}_{2b}, \vec{r}_{3b}) \psi(\vec{r}_{1a}) g_{et}(\hat{k}, \hat{q}_2) e^{ikq_2/q_2}, \quad (2.7)$$

as $q_2 \rightarrow \infty$,

where \mathcal{A} is the antisymmetrization operator; φ and ψ are the appropriate wave functions of H^- and H, respectively; q_1 and q_2 are the corresponding channel coordinates; f_s and g_{et} are the scattering and electron-transfer amplitudes; and

k is the asymptotic wave number for H^- and H.

For the electron-detachment channels, we have asymptotically two terms corresponding to the associative- and collisional-detachment channels¹⁶

$$p_3 \Upsilon \rightarrow \mathcal{A} \left\{ \sum_{\nu} \Psi_{\nu}(\vec{r}_1, \vec{r}_2, \vec{R}) g_{\nu}^{(ad)}(\hat{k}, \hat{q}_3) \frac{e^{i\kappa_{\nu} q_3}}{q_3} + \int dk_{\lambda} \rho_{k_{\lambda}} \psi(\vec{r}_{1a}) \psi(\vec{r}_{2b}) \chi_{k_{\lambda}}(\vec{R}) \times g_{\lambda}^{(cd)}(\hat{k}, \hat{q}_3) \frac{e^{i\kappa_{\lambda} q_3}}{q_3} \right\}, \quad \text{as } q_3 \rightarrow \infty, \quad (2.8)$$

where the Ψ_{ν} 's are the appropriate wave functions for H_2 ; q_3 is the channel coordinate for the detached electron (with respect to the c. m. of H^- and H); $g_{\nu}^{(ad)}$ and $g_{\lambda}^{(cd)}$ are the associative- and collisional-detachment amplitudes; κ_{ν} and κ_{λ} are the asymptotic wave numbers for the detached electrons in the associative- and collisional-detachment channels, respectively; and $\rho_{k_{\lambda}}$ is the density of the continuum states $\chi_{k_{\lambda}}(\vec{R})$ for H and H associated with the collisional-detachment channel.

The projectors p_1 , p_2 , and p_3 are constructed with the idempotent and orthogonal properties¹⁵

$$p_i p_j = p_j \delta_{ij}. \quad (2.9)$$

Though such projectors are required to be Hermitian only asymptotically,

$$p_j(q_j \rightarrow \infty) = p_j^+(q_j \rightarrow \infty), \quad (2.10)$$

Hermitian expressions may in certain cases be obtained for them.¹⁷ The P projection operator then takes the expression

$$P = p_1 + p_2 + p_3, \quad (2.11)$$

where the sum of the projectors are necessarily Hermitian. From Eqs. (2.9) and (2.11) it is clear that

$$p_j P = p_j, \quad p_j Q = p_j(1 - P) = 0. \quad (2.12)$$

Because the projectors, as well as the projection operator P , are defined only asymptotically, they are not unique in the near region of interaction, and may be constructed,¹⁷ for example, in terms of some suitably distorted (or polarized) functions which go over to the correct asymptotic unperturbed wave functions of the reactants and the products.

Operating Eq. (2.3) from the left-hand side with

the projector p_j , we obtain the following set of three coupled equations for the (H⁻, H) collision system:

$$\{E - \mathcal{K}_{p_j}\} p_j \Upsilon = \sum_{j' \neq j}^{j_0} \mathcal{K}_{p_j p_{j'}} p_{j'} \Upsilon, \quad j = 1, 2, \dots, j_0, \quad (2.13)$$

$$\text{with } \mathcal{K}_{p_j} = p_j \left\{ H + HQ \frac{1}{E - QHQ} QH \right\} p_j, \quad (2.14)$$

$$\mathcal{K}_{p_j p_{j'}} = p_j \left\{ H + HQ \frac{1}{E - QHQ} QH \right\} p_{j'}, \quad (2.15)$$

where we have used the idempotent and orthogonal properties of the projectors. On eliminating the electron-detachment channels in the set of coupled equations, we obtain a pair of coupled equations for scattering and electron-transfer channels

$$\left\{ E - \mathcal{K}'_{p_1} \right\} p_1 \Upsilon = \mathcal{K}'_{p_1 p_2} p_2 \Upsilon, \quad (2.16a)$$

$$\left\{ E - \mathcal{K}'_{p_2} \right\} p_2 \Upsilon = \mathcal{K}'_{p_2 p_1} p_1 \Upsilon, \quad (2.16b)$$

where

$$\mathcal{K}'_{p_i p_j} = \mathcal{K}_{p_i} \delta_{ij} + \mathcal{K}_{p_i p_3} \frac{1}{E - \mathcal{K}_{p_3} + i\epsilon} \mathcal{K}_{p_3 p_j}. \quad (2.17)$$

This pair of coupled equations, which are more convenient for dealing with scattering and electron-transfer collisions, are in principle equivalent to the set of three coupled equations. The detachment channels are now formally eliminated from the coupled equations, but are transformed into nonlocal energy-dependent complex channel potentials [see the second term in Eq. (2.17)] for the scattering and electron-transfer channels.

III. METHOD OF SOLUTION

The exact equations, Eqs. (2.16) or (2.13), are difficult to solve. In this section, we examine how these equations may be simplified with reasonable approximations, and how the simplified equations may be solved once certain approximate complex potentials become available for the effective channel potentials.

A. Born-Oppenheimer Separation Approximation

Utilizing the large mass disparity between the electrons and the nuclei, we may represent the channel wave functions $p_1 \Upsilon$ and $p_2 \Upsilon$ as products of the electronic and nuclear wave functions.

$$p_1 \Upsilon \cong \Phi_1(\vec{r}_1, \vec{r}_2, \vec{r}_3, \vec{R}) F(\vec{R}), \quad (3.1a)$$

$$p_2 \Upsilon \cong \Phi_2(\vec{r}_1, \vec{r}_2, \vec{r}_3, \vec{R}) G(\vec{R}), \quad (3.1b)$$

where Φ_1 and Φ_2 are the linear combinations of the appropriate Born-Oppenheimer electronic wave functions which go over to the atomic states $\alpha \varphi(\vec{r}_{1a}, \vec{r}_{2a}) \psi(\vec{r}_{3b})$ and $\alpha \varphi(\vec{r}_{2b}, \vec{r}_{3b}) \psi(\vec{r}_{1a})$, respectively, at large R ; and where F and G satisfy the asymptotic expressions that follow, respectively, from Eqs. (2.6) and (2.7), if one ignores certain recoil factors^{15, 17} which are negligibly small at low energies. In this approximation, we have neglected the small recoil factors and replaced the channel coordinates \vec{q}_1 and \vec{q}_2 by the internuclear coordinate \vec{R} .

Substitution of Eqs. (3.1) into (2.16) yields

$$\begin{aligned} \{K_{\vec{R}} + \langle \Phi_1 | \mathcal{K}'_{p_1} - K_{\vec{R}} P_1 | \Phi_1 \rangle - E\} F(\vec{R}) \\ = - \langle \Phi_1 | \mathcal{K}'_{p_1 p_2} | \Phi_2 \rangle G(\vec{R}), \end{aligned} \quad (3.2a)$$

$$\begin{aligned} \{K_{\vec{R}} + \langle \Phi_2 | \mathcal{K}'_{p_2} - K_{\vec{R}} P_2 | \Phi_2 \rangle - E\} G(\vec{R}) \\ = - \langle \Phi_2 | \mathcal{K}'_{p_2 p_1} | \Phi_1 \rangle F(\vec{R}), \end{aligned} \quad (3.2b)$$

where $K_{\vec{R}}$ is the kinetic-energy operator for the relative nuclear motion. This pair of coupled equations for F and G may be further simplified for the (H⁻, H) collision system when the symmetry of the identical nuclei is utilized.

B. Decoupling of the Pair Coupled Equations

We observe that Eqs. (3.2a) and (3.2b) for the scattering and resonant electron-transfer processes for the (H⁻, H) collision system are invariant under interchange of the two protons. This then allows a decoupling of these equations.

Upon interchange of the protons, we have for the electronic wave functions the property

$$\Phi_1(\vec{r}, \vec{R}) = \Phi_2(-\vec{r}, \vec{R}), \quad (3.3)$$

and for the projectors the property

$$p_j(\vec{r}, \vec{r}', \vec{R}) = p_j(-\vec{r}, -\vec{r}', \vec{R}), \quad (3.4)$$

where \vec{r} denotes the collection of the coordinates of the three electrons. This then implies that

$$\langle \Phi_1 | \mathcal{K}'_{p_1} - K_{\vec{R}} P_1 | \Phi_1 \rangle = \langle \Phi_2 | \mathcal{K}'_{p_2} - K_{\vec{R}} P_2 | \Phi_2 \rangle, \quad (3.5)$$

$$\langle \Phi_1 | \mathcal{K}'_{p_1 p_2} | \Phi_2 \rangle = \langle \Phi_2 | \mathcal{K}'_{p_2 p_1} | \Phi_1 \rangle, \quad (3.6)$$

which permit us to decouple Eqs. (3.2a) and (3.2b).

When Eqs. (3.3)–(3.6) are utilized, we obtain for Eqs. (3.2a) and (3.2b) the decoupled equa-

tions¹⁸

$$\{K_{\vec{R}} + V_{\pm}(\vec{R}) - \frac{1}{2}i\Gamma_{\pm}(\vec{R})\}\Xi_{\pm}(\vec{R}) = E\Xi_{\pm}(\vec{R}), \quad (3.7)$$

$$\text{where } \Xi_{\pm}(\vec{R}) = F(\vec{R}) \pm G(\vec{R}); \quad (3.8)$$

$$V_{\pm}(R) = \langle \Phi_i | \mathcal{K}_{p_i} - K_{\vec{R}} p_i | \Phi_i \rangle \\ + \text{Re}\{W_{\pm}\} - (1/2\mu) \langle \Phi_i | \nabla_{\vec{R}}^2 p_i | \Phi_i \rangle, \quad (3.9)$$

$$\Gamma_{\pm}(\vec{R}) = -2\text{Im}\{W_{\pm}\}; \quad (3.10)$$

$$W_{\pm}(\vec{R}) = \langle \Phi_i | \mathcal{K}_{p_i p_3} \frac{1}{E - \mathcal{K}_{p_3} + i\epsilon} \mathcal{K}_{p_3 p_i} | \Phi_i \rangle \\ \pm \langle \Phi_i | \mathcal{K}_{p_i p_3} \frac{1}{E - \mathcal{K}_{p_3} + i\epsilon} \mathcal{K}_{p_3 p_j} | \Phi_j \rangle. \quad (3.11)$$

In the Born-Oppenheimer separation approximation, the channel potentials are computed with the nuclei held fixed so that W_{\pm} may be treated as if it is local in R (see Sec. III C). We also assume that the energy dependence of the complex shifts W_{\pm} is weak, so that these quantities are determined by their values at the electronic resonance energies.

We seek solutions of Eq. (3.7) which behave asymptotically as

$$\Xi_{\pm}(\vec{R}) \rightarrow e^{ikR} + f_{\pm}(\hat{k} \cdot \hat{R})(e^{ikR}/R), \quad (3.12)$$

with

$$f_{\pm}(\hat{k} \cdot \hat{R}) = \frac{1}{2ik} \sum_l (2l+1) e^{2i\delta_l^{(\pm)}} (e^{-l} - 1) P_l(\cos\theta), \quad (3.13)$$

$$\delta_l^{(\pm)} = \zeta_l^{(\pm)} + i\eta_l^{(\pm)}, \quad (3.14)$$

where $\delta_l^{(\pm)}$ are the complex phase shifts of the radial parts of Eq. (3.7). The scattering and electron-transfer amplitudes can then be expressed in terms of f_{\pm} .¹⁸

$$P_1 \Upsilon = \frac{1}{2} \{ (p_1 + p_2) \Upsilon + (p_1 - p_2) \Upsilon \} - \alpha \varphi(\vec{r}_{1a}, \vec{r}_{2a}) \\ \times \psi(\vec{r}_{3b}) \{ e^{i\vec{k} \cdot \vec{R}} + \frac{1}{2}(f_+ + f_-) e^{ikR}/R \}, \text{ as } R \rightarrow \infty, \quad (3.15)$$

$$P_2 \Upsilon = \frac{1}{2} \{ (p_2 + p_2) \Upsilon - (p_1 - p_2) \Upsilon \} - \alpha \varphi(\vec{r}_{2b}, \vec{r}_{3b}) \\ \times \psi(\vec{r}_{1a}) \frac{1}{2} (f_+ - f_-) e^{ikR}/R, \text{ as } R \rightarrow \infty. \quad (3.16)$$

Hence, once the amplitudes f_+ and f_- are obtained, it is straightforward to calculate the process of scattering and electron transfer. From the imaginary part of the complex phase shifts (i. e., the $\eta_l^{(\pm)}$'s), the cross section for the detachment processes may be obtained.

C. Complex Channel Potential

The complex potential in Eq. (3.7) may be written in a symmetric form

$$V_{\pm}(\vec{R}) - i\frac{1}{2}\Gamma_{\pm}(\vec{R}) \\ = \langle \frac{1}{2}\sqrt{2} (p_1 \uparrow \Phi_1 \pm p_2 \uparrow \Phi_2) | \hat{\mathcal{K}} | \frac{1}{2}\sqrt{2} (p_1 \Phi_1 \pm p_2 \Phi_2) \rangle, \quad (3.17a)$$

$$\cong \langle \frac{1}{2}\sqrt{2} (p_1 \Phi_1 \pm p_1 \Phi_2) | \hat{\mathcal{K}} | \frac{1}{2}\sqrt{2} (p_1 \Phi_1 \pm p_2 \Phi_2) \rangle, \quad (3.17b)$$

$$\text{with } \hat{\mathcal{K}} = (\hat{H} - K_{\vec{R}}) + \hat{H} p_3 \frac{1}{E - p_3 \hat{H} p_3 + i\epsilon} p_3 \hat{H}, \quad (3.18)$$

$$\hat{H} = H + HQ \frac{1}{E - QHQ}, \quad (3.19)$$

where we have made use of Eqs. (3.5) and (3.6) and of the idempotent and orthogonal properties [Eq. (2.9)] of the projectors. The small Born-Oppenheimer correction term $-(1/2\mu) \langle \Phi_i | \nabla_{\vec{R}}^2 p_i | \Phi_i \rangle$ is neglected in Eq. (3.17) for simplicity. The inclusion of this term is straightforward.

Now if we replace \hat{H} by H (that is, if we neglect the closed-channel segment projected by Q), the first term in \hat{H} becomes simply the electronic part of the total Hamiltonian $H_e = H - K_R$. We have

$$\hat{H} \cong H_e + H p_3 \frac{1}{E - p_3 H p_3 + i\epsilon} p_3 H. \quad (3.20)$$

Since the functions $p_1 \Phi_1$ and $p_2 \Phi_2$ go over to the atomic states $\alpha \varphi(\vec{r}_{1a}, \vec{r}_{2a}) \psi(\vec{r}_{3b})$ and $\alpha \varphi(\vec{r}_{2b}, \vec{r}_{3b}) \psi(\vec{r}_{1a})$, respectively, at large R , the two linear combinations $p_1 \Phi_1 + p_1 \Phi_2$ and $p_1 \Phi_1 - p_1 \Phi_2$ possess the *gerade* and *ungerade* symmetry of molecular electronic states of the H_2^- molecule. It is then apparent that the first part of the complex potential, which is associated with the $(\hat{H} - K_R)$ part of Eq. (3.18), is simply the quasi-stationary potential [see Eq. (3.9)].

$$\mathcal{E}_{\pm}(\vec{R}) = \frac{1}{2} \langle p_1 \Phi_1 \pm p_2 \Phi_2 | H_e | p_1 \Phi_1 \pm p_2 \Phi_2 \rangle, \quad (3.21)$$

resulting from the electronic parts of the interaction between H^- and H in the *gerade* and *ungerade* modes.

The coupling with the electronic-detachment channel is given by the second term in Eq. (3.18). This coupling gives rise to the nonstationary character of the electronic interaction and intro-

duces into the quasistationary potential $\mathcal{E}(R)$ [Eq. (3.21)] complex shifts $W_{\pm}(R)$:

$$W_{\pm}(\vec{R}) \cong \frac{1}{2} \langle p_1 \Phi_1 \pm p_2 \Phi_2 | H p_3 \frac{1}{E - p_3 H p_3 + i\epsilon} \times p_3 H | p_1 \Phi_1 \pm p_2 \Phi_2 \rangle .$$

We emphasize that this complex shift is *nonlocal* and *energy-dependent*.

As an approximation, the energy dependence of W_{\pm} may be suppressed by evaluating W_{\pm} at a quasistationary energy $\mathcal{E}_{\pm}(\vec{R})$ for each value of R . In evaluating W_{\pm} , the nuclear motion may be held fixed. This then makes the complex shift $W_{\pm}(\vec{R})$ local. These approximations, of course, have a very restricted region of validity. It is apparent that if the energy of the system is increased, there will be more open channels to be included in P . Consequently, the complex shift $W_{\pm}(R)$ will be significantly modified. The non-local virtual excitation and polarization effects in the Q part [i. e., the $HQ(E - QHQ)^{-1}QH$ part] of Eq. (3.19) are also of importance and should be explicitly considered when the closed channels in Q become significantly coupled with the open channels of concern.

From this analysis it becomes clear that the channel potential may, for certain restricted regions, be approximated by a set of local energy-independent complex potentials. Several sets of complex potentials which are local and energy-independent have recently become available for the interaction between ground states of H⁻ and H. Although these potentials are of limited validity, it is nevertheless of interest to investigate the predictions of these potentials. In Fig. 1, these potentials are collected and compared for the real and imaginary parts. There are important differences among these potentials.

The set of theoretical complex potentials calculated by Bardsley, Herzenberg, and Mandl⁸ using an adiabatic stationary variational method¹⁹ is, in general, much larger than the set of semiempirical complex potentials determined by Chen and Peacher⁹ from dissociative-attachment measurements,^{20,21} including isotope effects. The theoretical and semiempirical results are in reasonable agreement for the real part of the *ungerade*-mode interaction. Experimental measurements^{22,23} on the vibrational excitation of H₂ molecules by electron impact indicate, however, that this part of interaction should be lower than

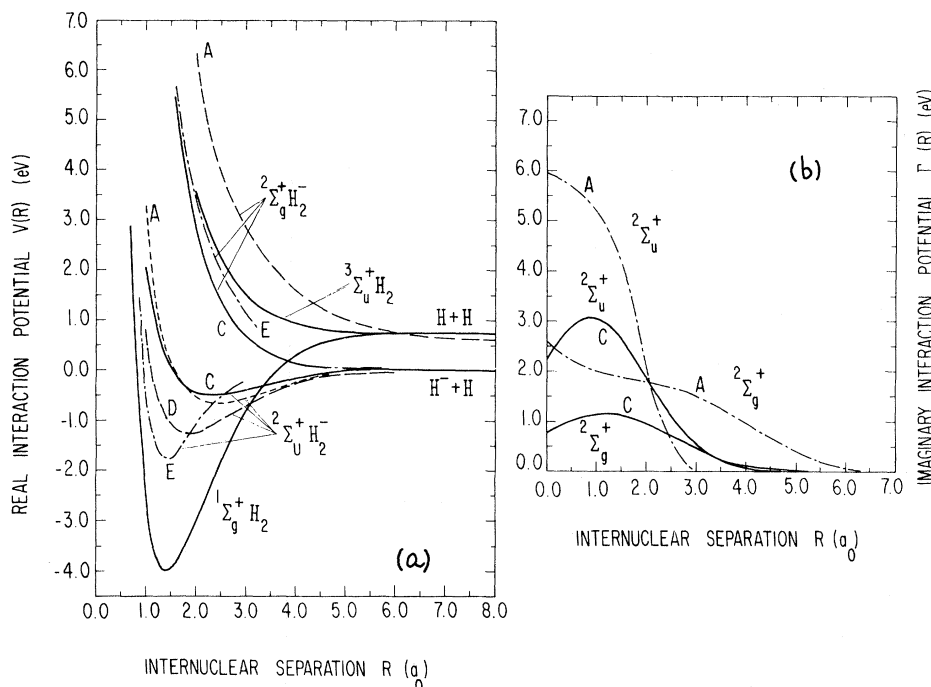


FIG. 1. Comparison of the complex potentials for the interaction between the ground states of H⁻ and H together with the $1\Sigma_g^+$ and $3\Sigma_u^+$ adiabatic potentials. Curves A, the $2\Sigma_g^+$ and $2\Sigma_u^+$ complex potentials calculated by Bardsley, Herzenberg, and Mandl (Ref. 8); curves C, the $2\Sigma_g^+$ and $2\Sigma_u^+$ complex potentials determined semiempirically by Chen and Peacher (Ref. 9); curves D, the modified real part of the $2\Sigma_u^+$ semiempirical complex potential (Ref. 17); curves E, the real parts of the $2\Sigma_g^+$ and $2\Sigma_u^+$ complex potentials calculated by Eliezer, Taylor, and Williams (Ref. 10). The $1\Sigma_g^+$ and $3\Sigma_u^+$ adiabatic potentials are calculated by Kolos and Wolniewicz [J. Chem. Phys. **43**, 2429 (1965)].

both the theoretical and semiempirical results. A modified semiempirical curve for the real part of the *ungerade*-mode interaction is obtained,¹⁷ and is shown in Fig. 1(a).

The real parts of the set of complex potentials have also been calculated by Eliezer, Taylor, and Williams,¹⁰ using an adiabatic stabilization method. The latter results do not agree with the real parts of the stationary variational results of Bardsley *et al.* The real part of the *gerade* mode interaction obtained by Eliezer *et al.*¹⁰ is, however, in reasonable agreement with the corresponding semiempirical curve. In view of the uncertainties in these potentials, we have carried out calculations using all these available potentials.

Six sets of complex potentials which go over to the appropriate long-range polarization potentials were constructed from these potentials. They are shown in Fig. 2. Sets A and B are the complex potentials calculated by Bardsley *et al.*⁸ In set B, the real part of the *gerade*-mode interaction (i. e., the ${}^2\Sigma_g^+H_2^-$ state) is modified in such a way that at large R , the system goes over to the correct energy states for H^- and H . Sets C and D are the semiempirical complex potentials. Set C is the semiempirical potential obtained by Chen and Peacher.⁹ Set D corresponds to the same set with the real part of the *ungerade* mode of interaction (i. e., the ${}^2\Sigma_u^+H_2^-$ states) modified¹⁷ in accordance with the vibrational-excitation measurements.^{22, 23} Sets E and F are constructed from the results of Eliezer *et al.*¹⁰ with the imaginary parts taken from the theoretical and the semiempirical complex potentials, respectively. The published curves of Eliezer *et al.* were given only for $R \leq 3a_0$. In sets E and F, their curves were extrapolated (somewhat arbitrarily) to the correct asymptotic energy states for H^- and H .

It should be noted that none of these potentials shown in Fig. 2 provides an adequate account of the physical system. The theoretical set of complex potentials (set A), and its modification (set B), do not yield values in agreement with dissociative-attachment and vibrational-excitation experiments.^{9, 24} These potentials, on the other hand, have been found³ to give reasonable agreement with electron-detachment experiments,²⁵ and to provide sufficient reduction in the cross section for the electron-transfer collisions²⁵ in an energy region $100\text{--}10^4$ eV. This is, however, a region where one expects that the nonadiabatic collisional detachment, which cannot be accounted for by these adiabatic potentials, would become significant. The semiempirical set of complex potentials (sets C and D) although accounting by construction for the dissociative-attachment and vibrational-excitation experiments, is certainly not unique. There is no reason to expect these potentials to have consistent accuracy for other

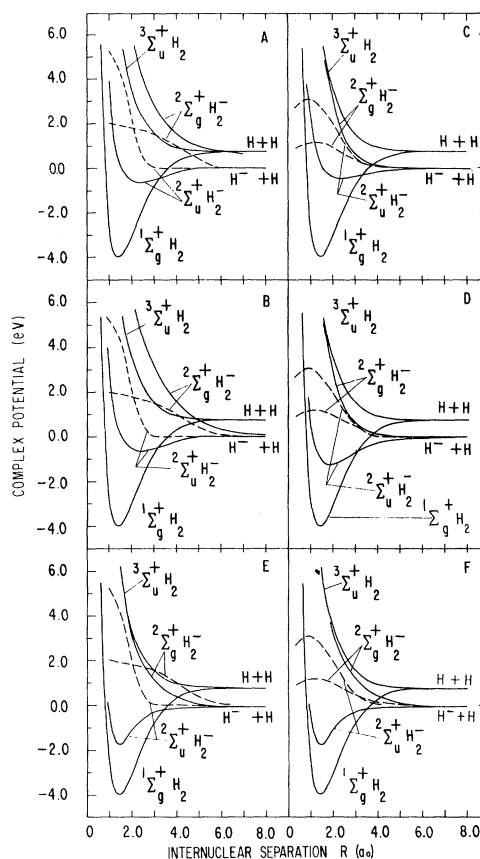


FIG. 2. Six model sets of complex potentials for the interaction between the ground states of H^- and H together with the ${}^1\Sigma_g^+$ and ${}^3\Sigma_u^+H_2$ adiabatic potentials. Set A, the complex potentials calculated by Bardsley, Herzenberg, and Mandl (Ref. 8); set B, the same as set A complex potentials but with the real part of the ${}^2\Sigma_g^+H_2^-$ potential modified to give asymptotically the correct energy states for H^- and H ; set C, the complex potentials determined semiempirically by Chen and Peacher (Ref. 9); set D, same as set C with the real part of the ${}^2\Sigma_u^+H_2^-$ potential replaced by curve D of Fig. 1; set E, the complex potentials constructed by combining the real parts calculated by Eliezer, Taylor, and Williams (Ref. 10) with the imaginary parts calculated by Bardsley, Herzenberg, and Mandl (Ref. 8); set F, the complex potentials constructed by combining the real parts calculated by Eliezer, Taylor, and Williams (Ref. 10) with the imaginary parts determined semiempirically by Chen and Peacher (Ref. 9). In sets E and F, the real parts of the potentials are extrapolated from the published curves at $R=3a_0$ (Ref. 10) to the correct asymptotic energy states for H^- and H .

processes, or at different energy regions. The complex potentials given by sets E and F, which are constructed by arbitrary combinations, have the same difficulties in comparison with experi-

ments.

Despite these inadequacies and the uncertainties in the long-range parts of the interaction between H⁻ and H, most of these sets of complex potentials should give correct predictions for the gross feature of the collision system. By a comparative study of these sets of complex potentials, one expects to obtain further insight into the role of electron detachment in (H⁻, H) collisions.

IV. RESULTS AND DISCUSSION

Application of Eq. (3.7) to the description of the (H⁻, H) collisions is carried out using the approximate $V_g(R) - \frac{1}{2}i\Gamma_g(R)$ and $V_u(R) - \frac{1}{2}i\Gamma_u(R)$ complex potentials shown in Fig. 2 for the $V_+ - \frac{1}{2}i\Gamma_+$ and $V_- - \frac{1}{2}i\Gamma_-$ decoupled channel potentials in the *gerade* - and *ungerade*-modes of interaction, respectively.

The radial collision wave functions are determined by solving the pair of equations

$$\left\{ \frac{d^2}{dR^2} - \frac{l(l+1)}{R^2} - 2\mu[E - V_g(R) + \frac{1}{2}i\Gamma_g(R)] \right\} \xi_l^{(g)}(R) = 0, \quad (4.1)$$

$$\left\{ \frac{d^2}{dR^2} - \frac{l(l+1)}{R^2} - 2\mu[E - V_u(R) + \frac{1}{2}i\Gamma_u(R)] \right\} \xi_l^{(u)}(R) = 0, \quad (4.2)$$

with the boundary conditions

$$\xi_l^{(g,u)}(R) \rightarrow k^{-1} \sin(kR - \frac{1}{2}l\pi + \delta_l^{(g,u)}), \text{ as } R \rightarrow \infty. \quad (4.3)$$

In the numerical calculation, the Numerov method is adopted for solving the differential equations. The complex phase shifts are determined by matching the numerical solutions with the asymptotical solutions at points outside of the range of the complex potentials.

A. Electron Survival Probability

For a reaction system with only four energetically accessible reaction paths as indicated by Eq. (2.1), the imaginary parts of the complex phase shifts determined from Eqs. (4.1) and (4.2) account entirely for the coupling with electron-detachment channels. (At energies below the detachment potential, the collisional-detachment channels are closed and electron detachment may proceed only through associative-detachment channels.) These imaginary phase shifts give rise to the damping of the nuclear motion and to the energy-dependent exponential factors

$$p_l^{(g,u)} = \exp[-2\text{Im}\delta_l^{(g,u)}] \quad (4.4)$$

in the expressions for scattering and electron-transfer cross sections [see Eqs. (4.33)–(4.36)].

Such an exponential factor has the physical significance of being the probability of electron detachment during the collision encounter. Such a survival probability factor has been suggested by Holstein²⁶ for the process of dissociative attachment (the reverse process of associative detachment), and later was verified by Bardsley, Herzenberg, and Mandl.²⁷

In Figs. 3 and 4, the calculated electron survival probability against electron detachment is shown as a function of relative angular momentum l for c. m. energies 0.005, 0.05, and 0.5 eV. It is seen that the six sets of complex potentials predict different behaviors for the survival probability. In addition to the dependence on the imaginary parts of the potential, the calculated values for $p_l^{(g,u)}$ also depend sensitively upon the changes in the real part of the complex potential when the imaginary parts are held unchanged.

For the *gerade* mode of interaction at low energies we observed that the theoretical complex potentials (i. e., sets A and B), despite the large imaginary potential, predict a much smaller electron-detachment probability than that predicted by the semiempirical complex potentials (i. e., set C). This is because the real part of the *gerade* potential in set B (or set A) at large distances is large, and prevents the low-energy colliding system from entering into the electron-detachment region. When the real part of the *gerade* potential in set B is replaced by that calculated by Eliezer *et al.*,¹⁰ as in set E, we find that the values for $p_l^{(g)}$ are reduced significantly, predicting a much larger electron detachment. The same replacement of the real part of the *gerade* potential in the semiempirical set results in an enhancement in the values for $p_l^{(g)}$. The net changes in $p_l^{(g)}$ appears, however, to be larger for set B than for set C, and more so as the energy of the system increases.

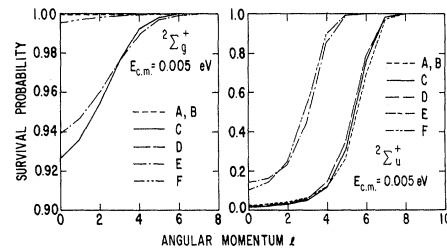


FIG. 3. Comparison of the electron-survival probability $p_l^{(g,u)}$ [Eq. (4.4)] in (H⁻, H) collisions as a function of the angular momentum l at c. m. energy 0.005 eV for the *gerade* and *ungerade* modes of interactions, as predicted by the six sets of complex potentials (see Fig. 2).

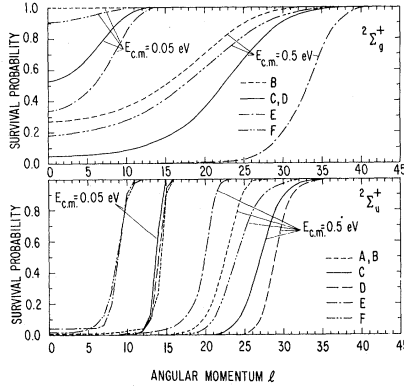


FIG. 4. Comparison of the electron-survival probability $p_l^{(g,u)}$ [Eq. (4.4)] in (H^-, H) collisions as a function of the angular momentum l at two c.m. energies for the *gerade* and *ungerade* modes of interactions as predicted by the sets B–F of complex potentials (see Fig. 2).

For the *ungerade* mode of interaction, the agreement in $p_l^{(u)}$, as predicted by the theoretical and semiempirical complex potentials, is reasonably good at low energies. Significant changes in $p_l^{(u)}$ are again observed when the real part of the *ungerade* potential is replaced by that calculated by Eliezer *et al.* These changes are, however, not as energy-dependent as for the *gerade* case.

The l dependence of the survival probability has been investigated by Chen and Peacher,²⁸ using the JWKB approximation for small l values. Their results, which were calculated on the basis of the potentials given by set B (and set A), are in good agreement with our results. We note that the survival probability approaches unity with increasing angular momentum l for each given energy. The rate of approach to unity decreases with increasing energy. This implies, of course, that as the energy increases, more partial waves should be included in the calculation of electron-detachment probabilities (or cross sections).

The energy dependence of the survival probability is investigated for fixed values of l . Some of the results for low l values are shown in Fig. 5 for set-B and set-C potentials. It is seen that at very low energies the behavior of the survival probability, predicted by the two sets of potentials, are essentially the same. Significant deviations are found in each l value as the energy is increased. The deviation is larger for the *gerade* mode of interaction than it is for the *ungerade* mode of interaction. As the energy is further increased, the survival probability approaches zero for each l value. The rate of approach to zero depends sensitively upon the potentials adopted in the calculations.

B. Scattering and Electron-Transfer Differential Cross Sections

Having obtained the complex phase shifts from Eqs. (4.1)–(4.3), the collision amplitudes due to each mode of interaction may be easily determined. Due to the symmetry with respect to the interchange of the protons in the (H^-, H) system, the angular-momentum quantum number l for the motion of the nuclei is limited to either even or odd values, according to the nuclear-spin symmetry, and the *gerade* and *ungerade* symmetries (the inversion symmetry) of the corresponding electronic states. The differential cross sections for the *gerade* and *ungerade* modes of interactions are then given, respectively, by

$$\frac{d\sigma_g^{(1,3)}}{d\Omega} = |f_g^{(1,3)}(\theta)|^2, \quad (4.5)$$

$$\frac{d\sigma_u^{(1,3)}}{d\Omega} = |f_u^{(1,3)}(\theta)|^2, \quad (4.6)$$

with the restricted sums

$$f_g^{(1)}(\theta) = \frac{1}{2ik} \sum_{l \text{ even}} (2l+1) \times \left(e^{2i\delta_l^{(g)}} - 1 \right) p_l(\cos\theta), \quad (4.7)$$

$$f_g^{(3)}(\theta) = \frac{1}{2ik} \sum_{l \text{ odd}} (2l+1)$$

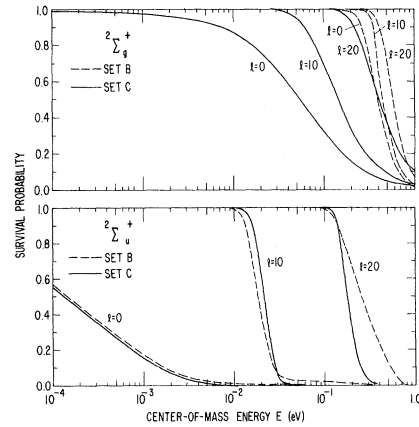


FIG. 5. Energy dependence of the electron-survival probability $p_l^{(g,u)}$ [Eq. (4.4)] in (H^-, H) collisions for angular momenta $l=0, 10,$ and 20 as predicted by set-B and set-C potentials (see Fig. 2).

$$\times \left(e^{2i\delta_l^{(g)}} - 1 \right) p_l(\cos\theta), \quad (4.8)$$

$$f_u^{(1)}(\theta) = \frac{1}{2ik} \sum_{l \text{ odd}} (2l+1) \times \left(e^{2i\delta_l^{(u)}} - 1 \right) p_l(\cos\theta), \quad (4.9)$$

$$f_u^{(3)}(\theta) = \frac{1}{2ik} \sum_{l \text{ even}} (2l+1) \times \left(e^{2i\delta_l^{(u)}} - 1 \right) p_l(\cos\theta), \quad (4.10)$$

where the superscripts (1) and (3) refer to the singlet and triplet nuclear-spin multiplicities of the (H⁻, H) collision system.

Since the *gerade* and *ungerade* modes of interaction are degenerate asymptotically, the elastic scattering and resonant electron-transfer amplitudes may be obtained from appropriate linear combinations of the collision amplitudes resulting from the *gerade* and the *ungerade* modes of interaction. This then gives rise to the interference in the scattering and electron-transfer differential cross sections. We have²⁹

$$\frac{d\sigma_s^{(1,3)}}{d\Omega} = \left\{ \frac{d\sigma_g^{(1,3)}}{d\Omega} + \frac{d\sigma_u^{(1,3)}}{d\Omega} + \frac{d\sigma_I^{(1,3)}}{d\Omega} \right\}, \quad (4.11)$$

$$\frac{d\sigma_{et}^{(1,3)}}{d\Omega} = \left\{ \frac{d\sigma_g^{(1,3)}}{d\Omega} + \frac{d\sigma_u^{(1,3)}}{d\Omega} - \frac{d\sigma_I^{(1,3)}}{d\Omega} \right\}, \quad (4.12)$$

where the interference contribution to the cross section is given by

$$\frac{d\sigma_I^{(1,3)}}{d\Omega} = 2\text{Re}(f_g^{(1,3)} f_u^{(1,3)*}). \quad (4.13)$$

The symbol Re denotes the real part of the quantity in the brackets.

For a random distribution of initial nuclear-spin orientations, the differential cross sections for any final spin orientation take the averaged expression for (H⁻, H) collisions

$$\frac{d\sigma_{s,et}}{d\Omega} = \frac{1}{4} \frac{d\sigma_{s,et}^{(1)}}{d\Omega} + \frac{3}{4} \frac{d\sigma_{s,et}^{(3)}}{d\Omega}. \quad (4.14)$$

A comparison of this averaged differential cross section, predicted by the six sets of complex potentials shown in Fig. 2, is given in Figs. 6-9 for five c. m. energies. The number of partial

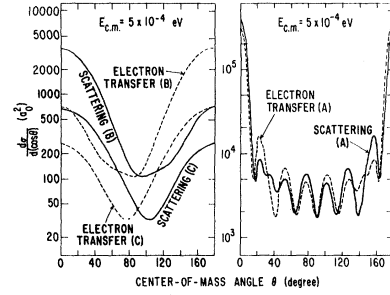


FIG. 6. Comparison of the differential scattering and electron-transfer cross sections [Eq. (4.14)] for the (H⁻, H) collision system as predicted by the sets A, B, and C of complex potentials (see Fig. 2) at an energy of 0.0005 eV in the c. m. system.

waves to be summed, in obtaining these results, increases rapidly with increasing energy and depends somewhat on the actual potential.

In Fig. 6, a comparison of the differential scattering and electron-transfer cross section, predicted by the potential sets A, B, and C, is shown for a c. m. energy of 0.0005 eV. It is seen that set-A potentials, because of the large tail of the *gerade* potential, predict a significantly larger cross section with rapid oscillations. These rapid oscillations may be removed if the tail of the *gerade* potential is reduced, so that it asymptotically goes over to the ground states of H and H⁻ as in set-B potentials. The behavior of the differential cross section for set-B and set-C potentials are very similar except that set B, because of the large splitting between the *gerade* and *ungerade* potentials, predicts somewhat larger differential cross sections.

As a result of the nuclear symmetry, the differential cross sections satisfy (see Fig. 6) the relation

$$\frac{d\sigma_s(\theta)}{d\Omega} = \frac{d\sigma_{et}(\pi-\theta)}{d\Omega}. \quad (4.15)$$

This permits us to deduce the differential cross sections, one from the other. We need not, therefore, present the differential cross sections over the entire range of the scattering angles.

A comparison of the scattering differential cross section as predicted by the sets of potentials B-F, (see Fig. 2) is given in Fig. 7 for a c. m. energy of 0.005 eV. It is seen that the oscillations in the differential cross section increase with increasing energy. Set-B potentials again predict larger differential cross sections than that predicted by the potentials of sets C-F. The change in the well depth in the real part of the semiempirical *ungerade* potential (compare set D with C) does not give rise to significant changes in the gross

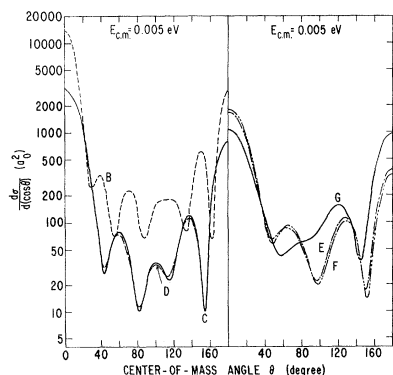


FIG. 7. Comparison of the differential scattering cross sections [Eq. (4.14)] for the (H^-, H) collision system as predicted by set B–F of complex potentials (see Fig. 2) at an energy of 0.005 eV in the c.m. system.

feature of the differential cross section.

The differences between the imaginary parts of the theoretical and semiempirical complex potentials do not appear to change the scattering and electron-transfer differential cross sections at these low energies. This can be seen from the comparison of the results between E and F sets of potentials in Fig. 7. As mentioned before, this behavior is due to the tail of the real part of *gerade* potential, which prevents the low-energy collision system from entering the electron-detachment region. Consequently, the collision system may enter the electron-detachment region only through the *ungerade* mode of interaction. The difference between the imaginary potentials should therefore appear due only to the *ungerade* parts. We have shown in Fig. 3 that at this low energy the *ungerade* imaginary phase shifts are large, and the survival probabilities $p_l^{(u)}$ predicted by the two sets of complex potentials are both very small, thus giving rise to large electron-detachment probabilities. Their differences are therefore not noticeable. However, if the imaginary parts of the complex potential is completely removed (i. e., set to zero) from set-E and set-F potentials, the significant changes indicated by curve G in Fig. 7 are observed.

Because the splitting between the real parts of the *gerade* and *ungerade* potentials calculated by Eliezer *et al.*¹⁰ is larger than that indicated by the semiempirical potentials, but smaller than that indicated by the theoretical potentials, set-E and set-F potentials predict a magnitude for the differential cross section which lies between sets B and C.

As energy is further increased, the collision system may enter the electron-detachment region in both modes of interactions. The difference between the imaginary parts of the theoretical and

semiempirical complex potentials becomes significant. This shown in Fig. 8. We observe that set F, with the semiempirical imaginary potential, gives rise to more damping in the interference oscillations, and that set E, with the theoretical imaginary potential, predicts smaller cross sections at and near the $\theta = 90^\circ$ collisions.

A comparison of the differential cross section predicted by B–D sets of complex potentials at somewhat higher energies is given in Fig. 9. It is seen that the differential cross section oscillates with increasing rapidity. These oscillations, which come primarily from the interference between the *gerade* and *ungerade* modes of collisions, are not symmetric. Part of the asymmetry comes from the rainbow scattering and the multipath interference in the *ungerade* mode of interaction. This is because the real part of the *gerade* potential has an attractive portion and changes its sign at certain characteristic internuclear separations. The nuclear symmetry also gives rise to interference which is appreciable at large angles. At small angles there is also diffraction-scattering (wave) interference coming from the second term in brackets of the collision amplitude [see Eqs. (4.7)–(4.10)].

Because the electron is flipping between the two hydrogen atoms while the collision encounter is taking place, the electron experiences different detachment potentials (imaginary potential) according to whether it is in the *gerade* or *ungerade* symmetries. Consequently, the oscillation in the *gerade-ungerade* interference will be damped with a different strength on each period of oscillation. This effect also accounts for some of the asymmetry in the oscillation shown in these figures.

To see the effect of the nuclear symmetry, the differential cross sections for scattering and electron-transfer are displayed in Figs. 10 and 11 for singlet and triplet collisions [Eqs. (4.11) and (4.12)] at c.m. energies 0.005 and 0.5 eV. We

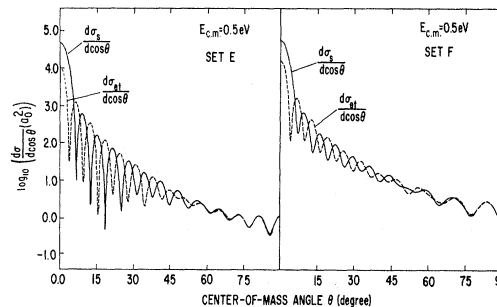


FIG. 8. Comparison of the differential scattering and electron-transfer cross sections [Eq. (4.14)] for the (H^-, H) collision system as predicted by the sets E and F of complex potentials (see Fig. 2) at an energy of 0.5 eV in the c.m. system.

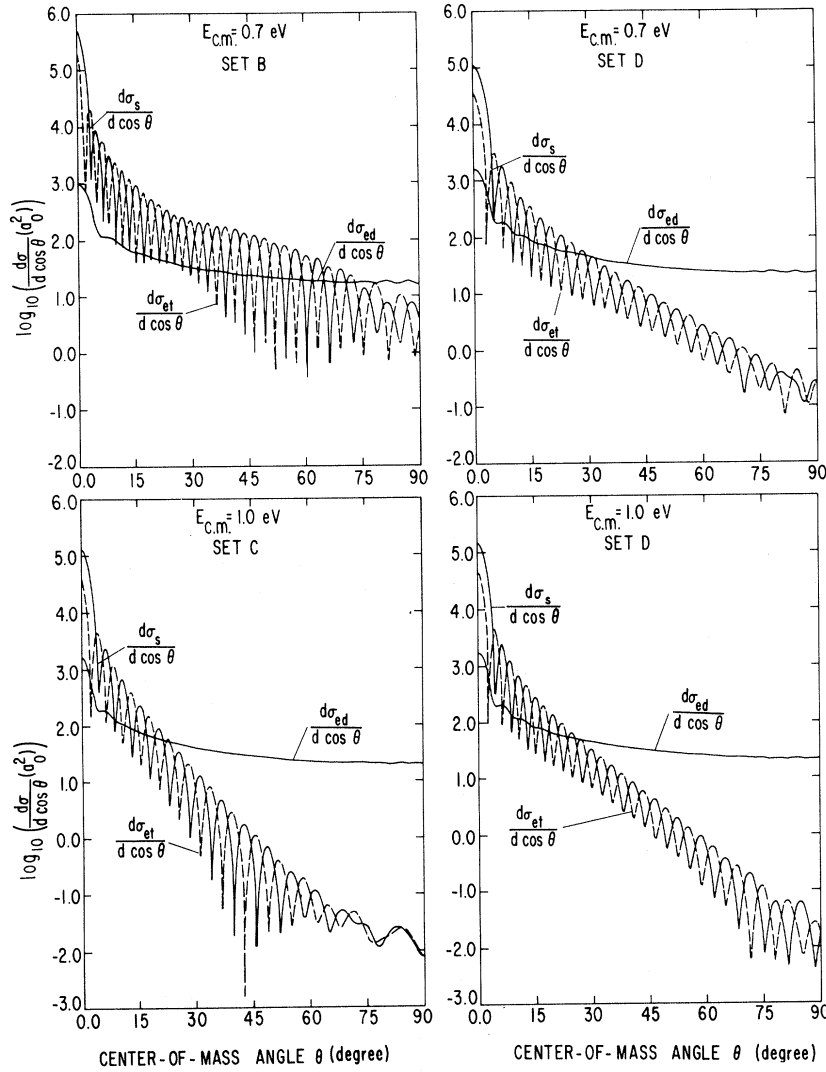


FIG. 9. Comparison of the differential scattering, electron-transfer, and electron-detachment cross sections [Eqs. (4.14) and (4.21)] for the (H^- , H) collision system as predicted by the sets B–D of complex potentials (see Fig. 2) at several energies in the c. m. system.

have included in these figures only the results obtained from the theoretical and semiempirical sets of complex potentials (sets B and C). It is seen that the singlet and triplet (H^- , H) collisions give rise to different *gerade-ungerade* oscillations (Fig. 10) due to differences in the nuclear-symmetry interference

$$f_g^{(1)}(\theta) = f_g^{(1)}(\pi - \theta), \quad f_u^{(1)}(\theta) = -f_u^{(1)}(\pi - \theta),$$

$$f_g^{(3)}(\theta) = -f_g^{(3)}(\pi - \theta), \quad f_u^{(3)}(\theta) = f_u^{(3)}(\pi - \theta).$$

At higher energies, the difference in the singlet and triplet *gerade-ungerade* oscillation pattern becomes noticeable only at large angles, as shown in Fig. 11. The diffraction interference remains unchanged.

For further details of the *gerade-ungerade* interference, these differential cross sections are decomposed in Figs. 12 and 13 into the *gerade*, *ungerade*, and their interference contributions [Eqs. (4.5), (4.6), and (4.13)] at c. m. energies 0.005 and 0.5 eV. As expected, the interference terms $d\sigma_I^{(1,3)}/d\Omega$ oscillate rapidly. Superimposed on the regular *gerade-ungerade* oscillations in $d\sigma_I^{(1,3)}/d\Omega$ are oscillations coming from the diffraction and nuclear-symmetry interferences and from interference within the *ungerade* collisions such as the multipath interference and rainbow scattering. It should be noted that the presence of a large imaginary potential can effectively damp the multipath interference and rainbow scattering. These effects would become more apparent if the nuclear symmetry were removed. This will be considered in Sec. IV F. By decomposing the scattering and electron-transfer differential cross sections into their components,

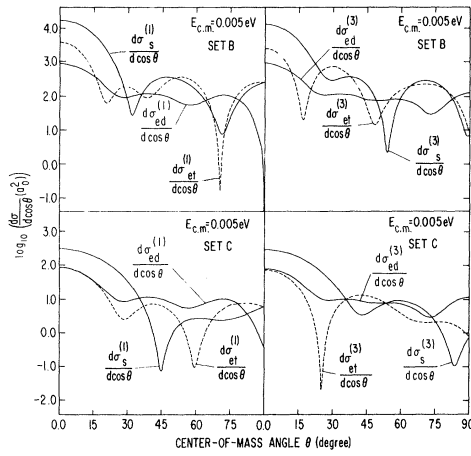


FIG. 10. Comparison of the singlet and triplet differential scattering, electron-transfer, and electron-detachment cross sections [Eqs. (4.11), (4.12), and (4.20)] for the (H^- , H) collision system as predicted by the sets B and C of complex potentials (see Fig. 2) at an energy of 0.005 eV in the c. m. system.

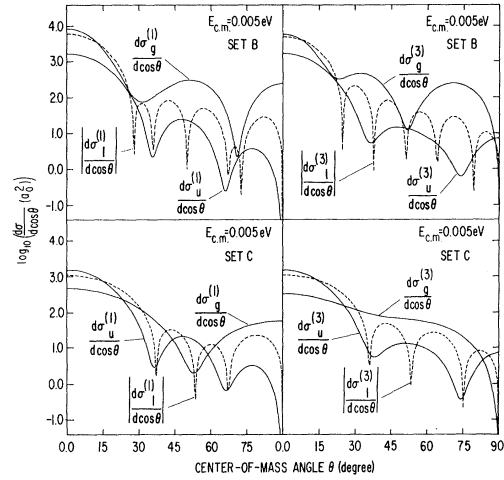


FIG. 12. Comparison of the *gerade*, *ungerade*, and their interference contributions [see Eqs. (4.5), (4.6), and (4.13)] to the singlet and triplet electron-transfer cross sections for the (H^- , H) collision system as predicted by the sets B and C of complex potentials (see Fig. 2) at an energy of 0.005 eV in the c. m. system.

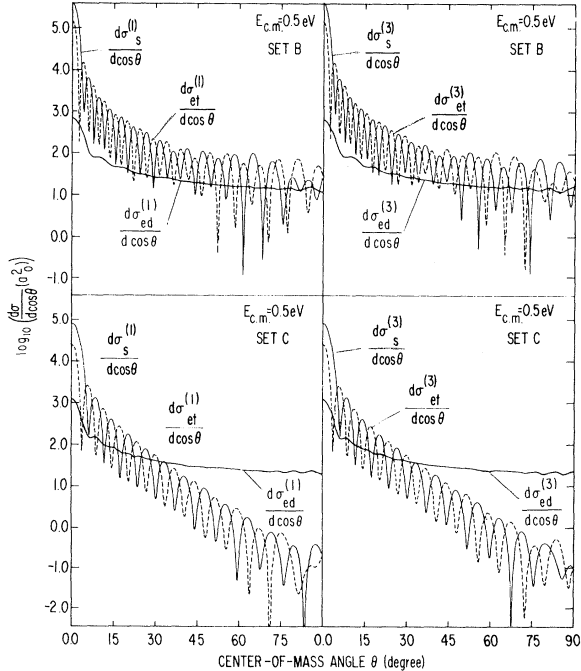


FIG. 11. Comparison of the singlet and triplet differential scattering, electron-transfer and electron-detachment cross sections [Eqs. (4.11), (4.12), and (4.20)] for the (H^- , H) collision system as predicted by the sets B and C of complex potentials (see Fig. 2) at an energy of 0.5 eV in the c. m. system.

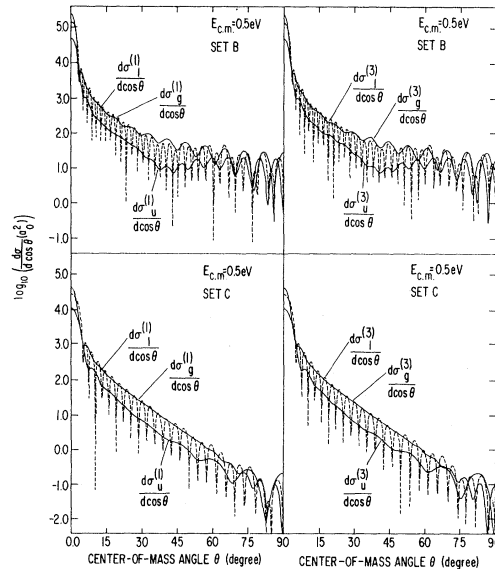


FIG. 13. Comparison of the *gerade*, *ungerade*, and their interference contributions [see Eqs. (4.5), (4.6), and (4.13)] to the differential scattering and electron-transfer cross sections for the (H^- , H) collision system as predicted by the sets B and C of complex potentials (see Fig. 2) at an energy of 0.5 eV in the c. m. system.

the diffraction interference at small angles now becomes more apparent. It is seen from Fig. 13 that the diffraction scattering occurs in the *gerade*-mode interaction at a smaller angle than in the *ungerade*-mode interaction.

C. "Differential" Electron-Detachment Cross Section

The cross section for electron detachment at a heavy-particle scattering angle θ (i.e., the angle between the incident-beam direction and the direction of the heavy-particle products) can be calculated from the imaginary parts of the complex phase shifts. The "differential" electron-detachment cross sections for the *gerade*- and the *ungerade*-mode interactions are given, with appropriate considerations of the nuclear symmetry, by the restricted sums

$$\frac{d\sigma_{\text{ed, g}}^{(1)}}{d\Omega} = \frac{1}{4k^2} \sum_{l \text{ even}} (2l+1)^2 \times \{1 - e^{-4\text{Im}\delta_l^{(g)}}\} p_l^2(\cos\theta), \quad (4.16)$$

$$\frac{d\sigma_{\text{ed, u}}^{(1)}}{d\Omega} = \frac{1}{4k^2} \sum_{l \text{ odd}} (2l+1)^2 \times \{1 - e^{-4\text{Im}\delta_l^{(u)}}\} p_l^2(\cos\theta), \quad (4.17)$$

$$\frac{d\sigma_{\text{ed, g}}^{(3)}}{d\Omega} = \frac{1}{4k^2} \sum_{l \text{ odd}} (2l+1)^2 \times \{1 - e^{-4\text{Im}\delta_l^{(g)}}\} p_l^2(\cos\theta), \quad (4.18)$$

$$\frac{d\sigma_{\text{ed, u}}^{(3)}}{d\Omega} = \frac{1}{4k^2} \sum_{l \text{ even}} (2l+1)^2 \times \{1 - e^{-4\text{Im}\delta_l^{(u)}}\} p_l^2(\cos\theta). \quad (4.19)$$

It is perhaps worthwhile to note that the word differential for the electron-detachment cross section does not have the conventional implications with respect to the scattering angle between the incident-beam direction and the direction of the electron detachment. The differential cross sections given by Eqs. (4.16)–(4.19) represent the cross sections for total electron detachment at a fixed solid-angle element $d\Omega$ for the heavy-particle

collisions. The word differential here refers therefore to the solid-angle element $d\Omega$. Such a differential cross section may be obtained from the double differential cross section for electron detachment,

$$\frac{d^2\sigma_{\text{ed}}^{(1,3)}(\theta, u, \epsilon_\lambda^{(g,u)})}{dwd\epsilon_\lambda^{(g,u)}},$$

by integrating over the electron-detachment solid-angle element dw and by summing (or integrating) over all the final heavy-particle states λ , taking appropriate account of the energy distribution of the detached electron associated with each λ (by integrating over $d\epsilon_\lambda^{(g,u)}$).

In Figs. 14 and 15 the differential electron-detachment cross sections for the *gerade* and *ungerade* modes of interaction are shown for c. m. energies 0.005 and 0.5 eV. It is seen that because of the nuclear symmetry, the cross sections oscillate almost exactly out of phase with each other at large angles. The relative contributions to the electron detachment from the *gerade* and *ungerade* modes of interaction changes significantly with the change in incident energy. The *gerade* contributions, because of the long tail in the *gerade* mode of interaction, become very small at low energies, and then, at higher energies, become comparable with the *ungerade* contributions. With further increase in energy, the collisional-detachment channel becomes open, and the *gerade* contribution eventually becomes larger than the *ungerade* contributions.

The total contribution to the singlet and triplet differential electron-detachment cross section is then given by

$$\frac{d\sigma_{\text{ed}}^{(1,3)}}{d\Omega} = \frac{d\sigma_{\text{ed, g}}^{(1,3)}}{d\Omega} + \frac{d\sigma_{\text{ed, u}}^{(1,3)}}{d\Omega}. \quad (4.20)$$

The averaged differential detachment cross section over final spin state may then be obtained:

$$\frac{d\sigma_{\text{ed}}}{d\Omega} = \frac{1}{4} \frac{d\sigma_{\text{ed}}^{(1)}}{d\Omega} + \frac{3}{4} \frac{d\sigma_{\text{ed}}^{(3)}}{d\Omega}. \quad (4.21)$$

A comparison of this averaged differential electron-detachment cross section as predicted by the various sets of complex potentials is given in Fig. 16 for c. m. energies 0.005 and 0.5 eV. Some of the higher-energy results are shown in Fig. 9. Due to the absence of the *gerade*-*ungerade* oscillations, the structure in the differential detachment cross section comes from the *ungerade*-mode collisions and from the nuclear symmetry and

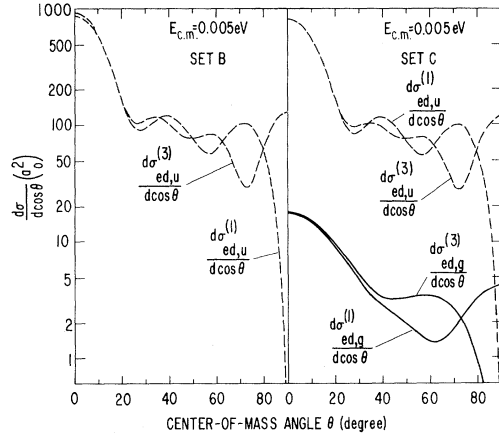


FIG. 14. *Gerade* and *ungerade* contributions to the differential electron-detachment cross section for singlet and triplet (H^- , H) collisions [Eqs. (4.16)–(4.19)] as predicted by the sets B and C of complex potentials (see Fig. 2) at an energy of 0.005 eV in the c.m. system.

diffraction scatterings. The singlet and triplet components of the cross section (Fig. 16) are shown in Figs. 10 and 11.

From Figs. 10 and 11, it is seen that the detachment cross section depends not only on the imaginary parts of the potentials, but also sensitively on the real parts of the potentials. This behavior is expected from the observations made on the electron-survival probability in Sec. IV A. At higher energies, the dependence on the real

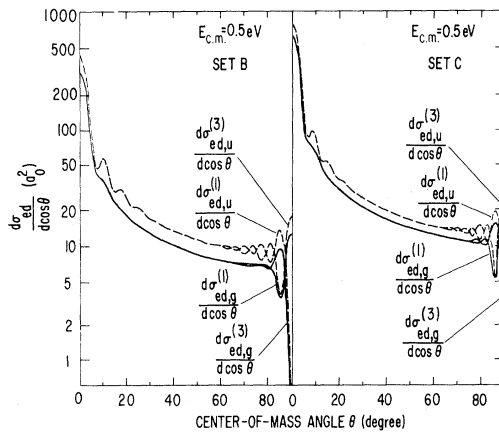


FIG. 15. *Gerade* and *ungerade* contributions to the differential electron-detachment cross section for singlet and triplet (H^- , H) collisions [Eqs. (4.16)–(4.19)] as predicted by the sets B and C of complex potentials (see Fig. 2) at an energy of 0.5 eV in the c.m. system.

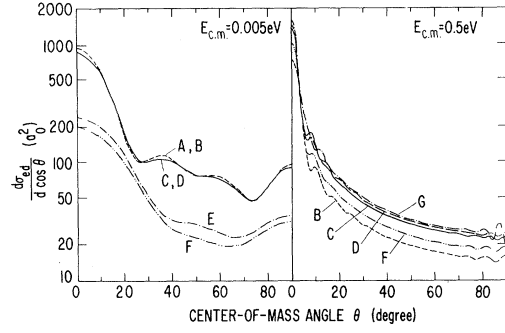


FIG. 16. Comparison of the differential electron-detachment cross sections [Eq. (4.21)] for the (H^- , H) collision system as predicted by the sets A–F of complex potentials (see Fig. 2) at energies of 0.005 and 0.5 eV in the c.m. system.

parts of the potentials becomes less sensitive.

The averaging of the differential detachment cross section over the final-spin orientation may also be done for the *gerade* and *ungerade* contributions separately:

$$\frac{d\sigma_{ed}^{(g)}}{d\Omega} = \frac{1}{4} \frac{d\sigma_{ed,g}^{(1)}}{d\Omega} + \frac{3}{4} \frac{d\sigma_{ed,u}^{(3)}}{d\Omega}, \quad (4.22)$$

$$\frac{d\sigma_{ed}^{(u)}}{d\Omega} = \frac{1}{4} \frac{d\sigma_{ed,u}^{(1)}}{d\Omega} + \frac{3}{4} \frac{d\sigma_{ed,u}^{(3)}}{d\Omega}. \quad (4.23)$$

Equation (4.21) may then be rewritten

$$\frac{d\sigma_{ed}}{d\Omega} = \frac{d\sigma_{ed}^{(g)}}{d\Omega} + \frac{d\sigma_{ed}^{(u)}}{d\Omega}. \quad (4.24)$$

The comparison of the averaged *gerade* and *ungerade* differential detachment cross sections is given in Fig. 17 for a c.m. energy 0.005 eV. These spin-averaged *gerade* and *ungerade* cross sections are useful for the investigation of isotope effects (Sec. IV F).

D. Electron-Detachment and Electron-Transfer Probabilities

Having determined the differential cross section, the electron-detachment probability P_{ed} and the electron-transfer probability P_{et} can be calculated from the relations

$$P_{ed} = \left(\frac{d\sigma_{ed}}{d\Omega} \right) / \left(\frac{d\sigma_{total}}{d\Omega} \right), \quad (4.25)$$

$$P_{et} = \left(\frac{d\sigma_{et}}{d\Omega} \right) / \left(\frac{d\sigma_{total}}{d\Omega} \right), \quad (4.26)$$

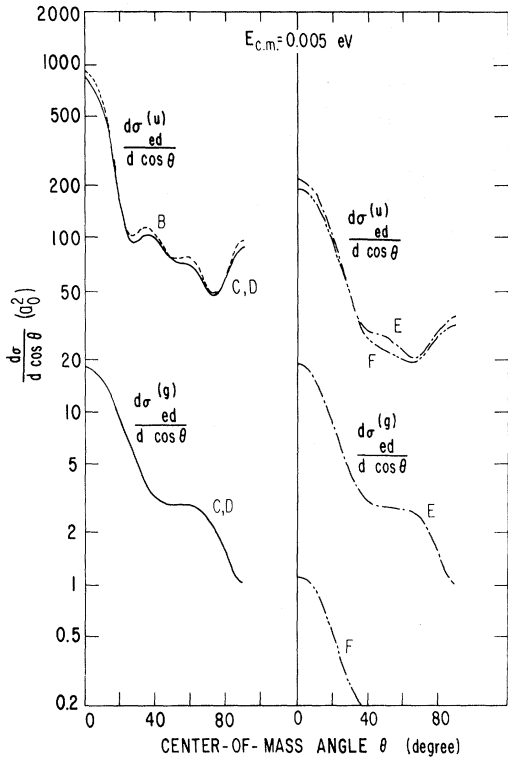


FIG. 17. Comparison of the spin orientation averaged *gerade* and *ungerade* contributions to the differential electron-detachment cross section [Eqs. (4.22) and (4.23)] for the (H⁻, H) collision system as predicted by the sets B–F of complex potentials at an energy of 0.005 eV in the c. m. system.

where $d\sigma_{\text{total}}/d\Omega$ is the total differential cross section for the (H⁻, H) collision system. For energies below the excitation thresholds of the hydrogen atom, the total differential cross section is given by

$$\frac{d\sigma_{\text{total}}}{d\Omega} = \frac{d\sigma_{\text{s}}}{d\Omega} + \frac{d\sigma_{\text{et}}}{d\Omega} + \frac{d\sigma_{\text{ed}}}{d\Omega} \quad (4.27)$$

Some of the calculated P_{ed} and P_{et} are displayed in Figs. 18–20 as functions of the c. m. scattering angle θ for several c. m. energies, and in Figs. 21 and 22 as functions of the c. m. energies for several c. m. scattering angles.

From Fig. 18 it is seen that the change in well depth in the real part of the *ungerade* potential from sets C to D does not give rise to appreciable changes in P_{et} and P_{ed} at these low energies. As noted before, at this low energy the collision system may enter the electron-detachment region only along the *ungerade* mode of interaction. To see the damping effect due to the *ungerade* imaginary potential, the electron-transfer probability

was calculated using set-E (or set-F) potentials without the imaginary parts. The result is shown in Fig. 18 as curve G. The damping due to electron detachment is clearly very significant in both the scattering and electron-transfer probabilities. Such damping, unlike the damping due to coupling with the H-excitation channels, is of importance for collisions involving negative ions.

The electron-detachment probability P_{ed} which is symmetric with respect to the 90° axis, is found to peak at $\theta = 90^\circ$. This peaking at 90° becomes more significant at higher energies. From Figs. 19 and 20, it is seen that at $\theta = 90^\circ$ the probability for electron-transfer and scattering, except for set-B potentials, is negligibly small in comparison with the probability of electron detachment. This then suggests that for experimental study of electron ejection in heavy-particle collisions it would be more advantageous to carry out the measurement at a large angle with respect to the beam direction. From Fig. 9 we have seen that the magnitude of the detachment cross section does not decrease appreciably with increasing angle θ .

The energy dependence of the electron-transfer probability is shown in Fig. 21 for small-angle collisions. Though the probability of electron detachment is small at these small-angle collisions, their effect on electron-transfer probability is already noticeable. The oscillations for P_{et} shown in Fig. 21 do not extend from zero to unity as they build up with increasing angles. Such damping due to electron detachment is characteristic of elec-

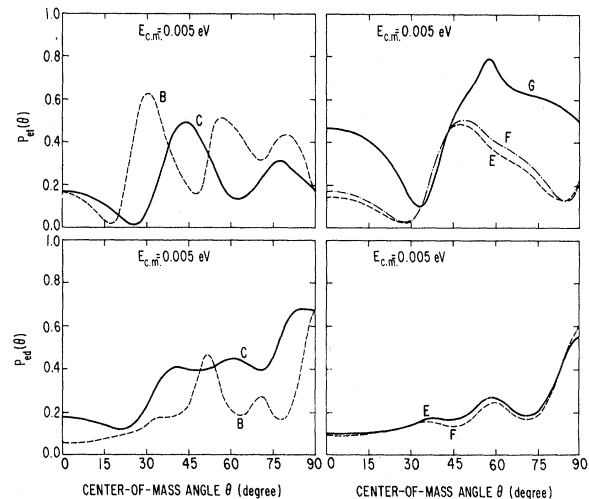


FIG. 18. Comparison of the electron-transfer and electron-detachment probabilities [Eqs. (4.25) and (4.26)] in (H⁻, H) collision as predicted by the sets B–F of complex potentials (see Fig. 2) at a c. m. energy of 0.005 eV. Curve G is obtained from set E (and set F) without the imaginary parts of the potentials.

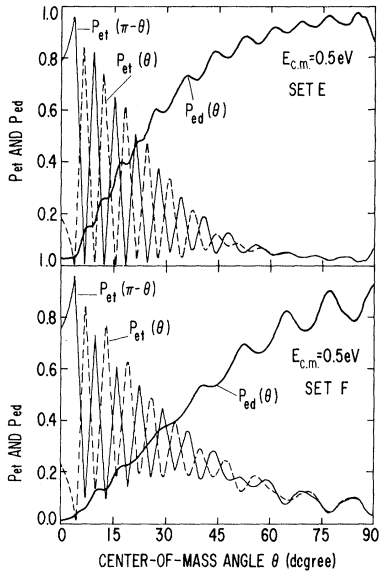


FIG. 19. Comparison of the electron-transfer and electron-detachment probabilities [Eqs. (4.25) and (4.26)] in (H^-, H) collisions as predicted by the sets E and F of complex potentials (see Fig. 2) at a c.m. energy of 0.5 eV.

tron-transfer problems involving negative ions. From Figs. 9, 19, and 20, it is evident that the electron-detachment damping would become more

apparent with increasing θ . The energy dependence of the electron-detachment probability is given in Fig. 22. It is seen that in low-energy regions the probability of electron detachment does not change appreciably with energy.

It is obvious that if the final nuclear-spin orientations are specified, the electron-detachment and electron-transfer probabilities may be defined for each spin multiplicity:

$$P_{et}^{(1,3)} = \left(\frac{d\sigma_{ed}^{(1,3)}}{d\Omega} \right) / \left(\frac{d\sigma_{total}^{(1,3)}}{d\Omega} \right), \quad (4.28)$$

$$P_{et}^{(1,3)} = \left(\frac{d\sigma_{et}^{(1,3)}}{d\Omega} \right) / \left(\frac{d\sigma_{total}^{(1,3)}}{d\Omega} \right), \quad (4.29)$$

with

$$\frac{d\sigma_{total}^{(1,3)}}{d\Omega} = \frac{d\sigma_s^{(1,3)}}{d\Omega} + \frac{d\sigma_{et}^{(1,3)}}{d\Omega} + \frac{d\sigma_{ed}^{(1,3)}}{d\Omega}, \quad (4.30)$$

where the singlet and triplet differential cross sections for scattering, electron-transfer, and electron-detachment are given by Eqs. (4.11), (4.12), and (4.20), respectively.

A comparison of the electron-detachment and electron-transfer probabilities in the singlet and triplet (H^-, H) collisions is given in Figs. 23 and 24. The differences are significant for low ener-

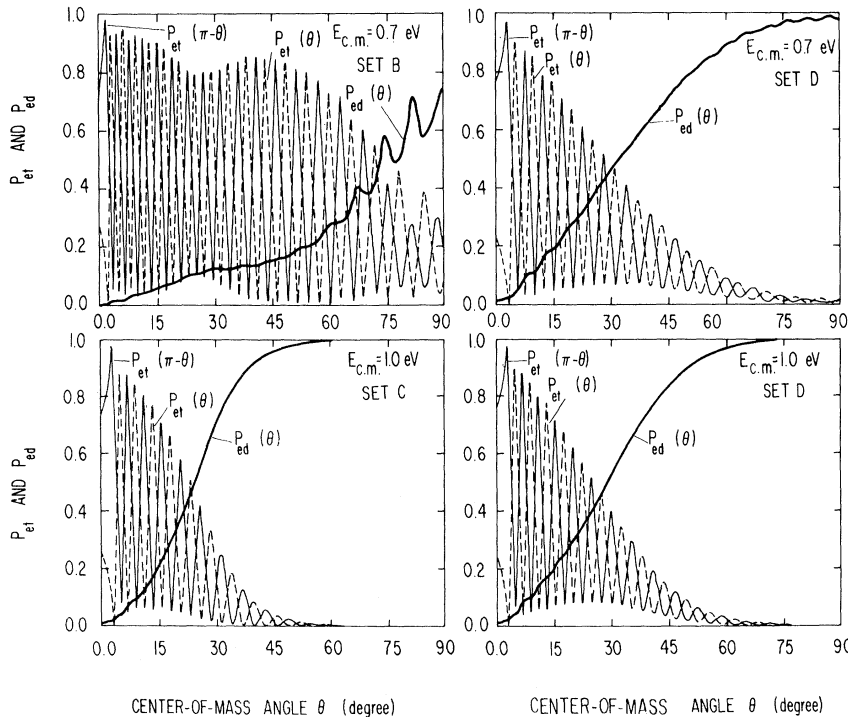


FIG. 20. Comparison of the electron-transfer and electron-detachment probabilities [Eqs. (4.25) and (4.26)] in (H^-, H) collisions as predicted by B and D sets of complex potentials (see Fig. 2) at c.m. energy 0.7 eV and by the sets C and D of complex potentials (see Fig. 2) at c.m. energy 1.0 eV.

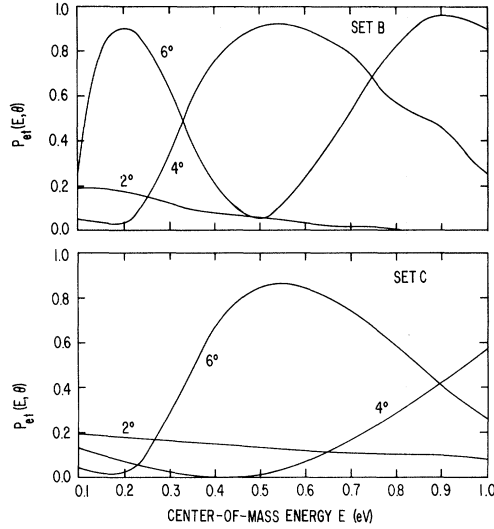


FIG. 21. Comparison of the energy dependence of the electron-transfer probability [Eq. (4.26)] in (H^- , H) collisions at c.m. angles 2° , 4° , and 6° as predicted by the sets B and C of complex potentials (see Fig. 2).

gies. From Fig. 23, it is seen that the electron-detachment probability in the singlet (H^- , H) collisions is no longer peaked at $\theta = 90^\circ$. This is again related to the fact that, at low energies, the *ungerade* mode dominates the detachment. At higher energies, the difference between the singlet

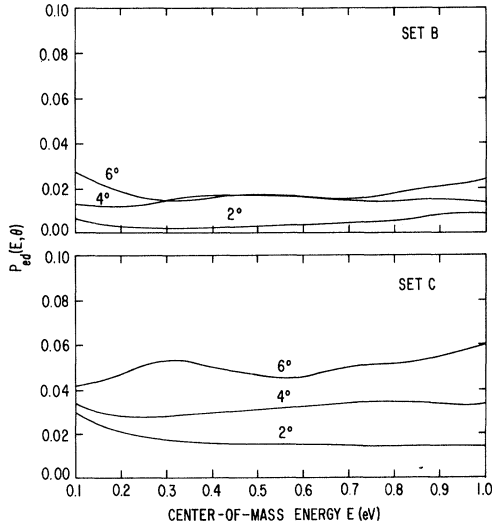


FIG. 22. Comparison of the energy dependence of the electron-detachment probability [Eq. (4.26)] in (H^- , H) collisions at c.m. angles 2° , 4° , and 6° as predicted by the sets B and C of complex potentials (see Fig. 2).

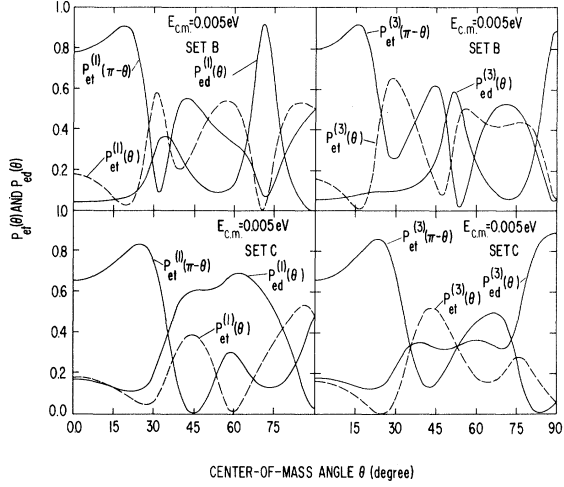


FIG. 23. Comparison of the electron-transfer and electron-detachment probabilities for singlet and triplet (H^- , H) collisions [Eqs. (4.28) and (4.29)] as predicted by the sets B and C of complex potentials (see Fig. 2) at a c.m. energy of 0.005 eV.

and triplet behavior becomes small.

E. Total Cross Section

The total scattering or electron-transfer cross section can be obtained from Eq. (4.15) by integrating over $d\Omega$. The interference between the *gerade* and *ungerade* contributions in Eqs. (4.11) and (4.12) vanishes on integration. Consequently, the total scattering and the total electron-transfer cross section become identical and are simply given by the sum of the *gerade* and *ungerade* contributions.

$$\sigma_{s,et} = \sigma_g + \sigma_u \quad (4.31)$$

For any final nuclear-spin orientation σ_g and σ_u is given by

$$\sigma_{g,u} = \frac{1}{4}\sigma_{g,u}^{(1)} + \frac{3}{4}\sigma_{g,u}^{(3)}, \quad (4.32)$$

$$\text{with } \sigma_g^{(1)} = \frac{4\pi}{k^2} \sum_{l(\text{even})} (2l+1) e^{-2\text{Im}\delta_l^{(g)}} \times \{ \sin^2[\text{Re}\delta_l^{(g)}] + \sinh^2[\text{Im}\delta_l^{(g)}] \}, \quad (4.33)$$

$$\sigma_u^{(1)} = \frac{4\pi}{k^2} \sum_{l(\text{odd})} (2l+1) e^{-2\text{Im}\delta_l^{(u)}} \times \{ \sin^2[\text{Re}\delta_l^{(u)}] + \sinh^2[\text{Im}\delta_l^{(u)}] \}, \quad (4.34)$$

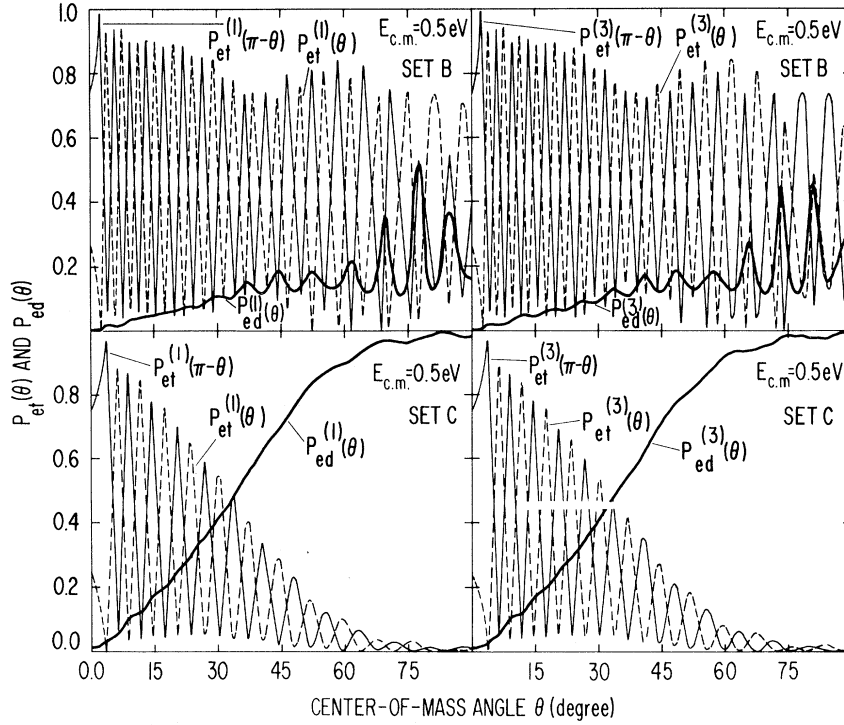


FIG. 24. Comparison of the electron-transfer and electron-detachment probabilities for singlet and triplet (H^- , H) collisions [Eqs. (4.28) and (4.29)] as predicted by the sets B and C of complex potentials (see Fig. 2) at a c.m. energy of 0.5 eV.

$$\sigma_g^{(3)} = \frac{4\pi}{k^2} \sum_{l(\text{odd})} (2l+1) e^{-2\text{Im}\delta_l^{(g)}} \times \{ \sin^2[\text{Re}\delta_l^{(g)}] + \sinh^2[\text{Im}\delta_l^{(g)}] \}, \quad (4.35)$$

$$\sigma_u^{(3)} = \frac{4\pi}{k^2} \sum_{l(\text{even})} (2l+1) e^{-2\text{Im}\delta_l^{(u)}} \times \{ \sin^2[\text{Re}\delta_l^{(u)}] + \sinh^2[\text{Im}\delta_l^{(u)}] \}, \quad (4.36)$$

In Fig. 25, a comparison of the total scattering cross section, predicted by set-B and set-C complex potentials, is given. It is seen that, as a result of the large splitting between the *gerade* and *ungerade* modes of interaction, set B predicts a much larger cross section than set C. For further details, the *gerade* and *ungerade* contributions [Eq. 4.32] to $\sigma_{S,et}$ are also included in Fig. 25. The difference in the magnitude of the cross section results primarily from the *gerade* contributions.

Because the *gerade-ungerade* interference term is absent, the cross section becomes a smooth function of energy. At very low energies, the scattering cross section exhibits, nevertheless, interesting structures, as shown in Fig. 26. To see the origin of this structure, the *gerade* and *ungerade* contributions to the singlet and triplet (H^- , H) collisions are shown in Fig. 27. It is seen that the *gerade*, as well as the *ungerade*,

contributions to the singlet and triplet collisions become oscillating with increasing rapidity as energy decreases. These oscillations, being almost exactly out of phase with each other, would be canceled if the *gerade* and *ungerade* contributions were to be summed with equal weights. Because the triplet contribution weighs statistically more than the singlet contribution, the oscillations are not canceled. This gives rise to the structure in the total scattering cross section at low energies.

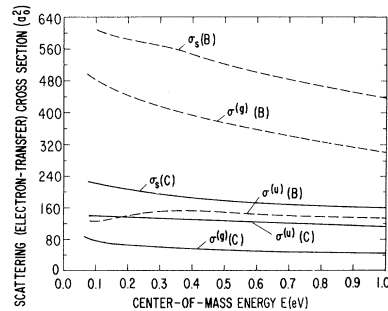


FIG. 25. Comparison of the scattering (or electron-transfer) cross section [Eqs. (4.31)] and its *gerade* and *ungerade* contributions [Eqs. (4.32)] as functions of energy for the (H^- , H) collision system as predicted by the sets B and C of complex potentials (see Fig. 2) in the c.m. system.

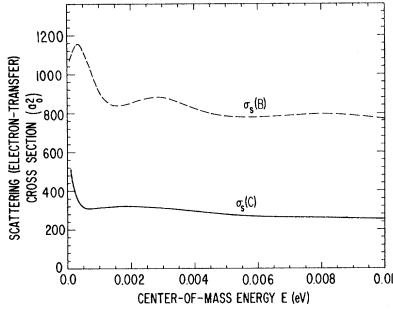


FIG. 26. Comparison of the scattering (electron-transfer) cross sections [Eq. (4.31)] as a function of energy for the (H⁻, H) collision system as predicted by the sets B and C of complex potentials (see Fig. 2) in the c.m. system.

The total electron-detachment cross section can be obtained from Eq. (4.21) [or (4.24)] simply by integrating over $d\Omega$. We have

$$\sigma_{ed} = \sigma_{ed}^{(g)} + \sigma_{ed}^{(u)}, \quad (4.37)$$

$$\text{with } \sigma_{ed}^{(g)} = \frac{1}{4}\sigma_{ed,g}^{(1)} + \frac{3}{4}\sigma_{ed,g}^{(3)}, \quad (4.38)$$

$$\sigma_{ed}^{(u)} = \frac{1}{4}\sigma_{ed,u}^{(1)} + \frac{3}{4}\sigma_{ed,u}^{(3)}, \quad (4.39)$$

where the *gerade* and *ungerade* contributions to electron detachment in the singlet and triplet (H⁻, H) collisions are given by

$$\sigma_{ed,g}^{(1)} = \frac{\pi}{k^2} \sum_{l(\text{even})} (2l+1) \{1 - e^{-4 \text{Im}\delta_l^{(g)}}\}, \quad (4.40)$$

$$\sigma_{ed,u}^{(1)} = \frac{\pi}{k^2} \sum_{l(\text{odd})} (2l+1) \{1 - e^{-4 \text{Im}\delta_l^{(u)}}\}, \quad (4.41)$$

$$\sigma_{ed,g}^{(3)} = \frac{\pi}{k^2} \sum_{l(\text{odd})} (2l+1) \{1 - e^{-4 \text{Im}\delta_l^{(g)}}\}, \quad (4.42)$$

$$\sigma_{ed,u}^{(3)} = \frac{\pi}{k^2} \sum_{l(\text{even})} (2l+1) \{1 - e^{-4 \text{Im}\delta_l^{(u)}}\}. \quad (4.43)$$

The total electron-detachment cross section and its constituent *gerade* and *ungerade* contributions are shown in Fig. 28 for set-B and set-C complex potentials. At these energies, set C predicts a larger cross section for electron detachment than set B. This is just the reverse situation from the

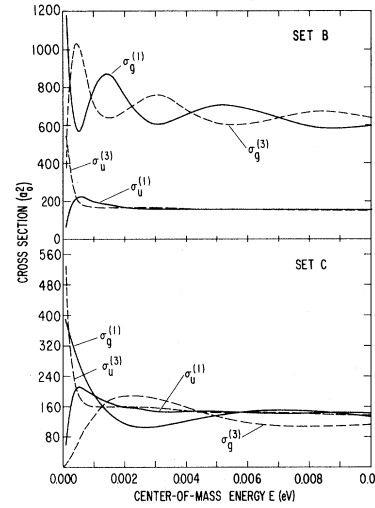


FIG. 27. *Gerade* and *ungerade* contributions to the scattering (electron-transfer) cross section [Eqs. (4.33)–(4.36)] for the singlet and triplet (H⁻, H) collisions as a function of energy as predicted by the sets B and C of complex potentials (see Fig. 2) in the c.m. system.

scattering cross section. The reason for this behavior is again due to the large *gerade*-potential tail. As the energy of the colliding system is increased, the *gerade* contribution to electron detachment for set-B potentials increases rapidly and pushes the total detachment cross section up to that predicted by set-C potentials. As energy is increased further, set-B potentials predict a larger detachment cross section than do

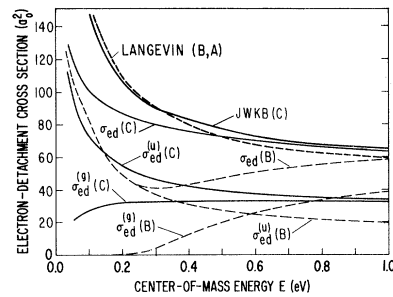


FIG. 28. Comparison of the total electron-detachment cross section [Eq. (4.37)] and its *gerade* and *ungerade* contributions [Eqs. (4.38) and (4.39)] as functions of energy for the (H⁻, H) collision system as predicted by the sets B and C of complex potentials (see Fig. 2) in the c.m. system. The curve labeled JWKB and Langevin are predicted by set-C and set-B potentials in the JWKB approximation (Ref. 32) and the Langevin spiral approximation (Ref. 3), respectively.

set-C potentials. The result of our investigation of (H^- , H) collisions at high-energy regions will be reported in a subsequent paper.

For comparison, we have included in Fig. 28 the result of previous calculations^{2,30} using the Langevin spiraling and JWKB approximations. The JWKB result was calculated using set-C potentials, while the Langevin spiraling result was estimated based on set-B (or set-A) potentials. It is seen that both the JWKB and the Langevin spiraling approximations give reasonable agreement with the numerical cross section.

In Fig. 29 the very low-energy results for the electron-detachment cross section are shown. In this low-energy region the *gerade* contribution is negligibly small, and the differences between set-B and set-C potentials are small. The structure in the total detachment cross section results again from the residual oscillations in the *ungerade* contributions to the electron detachment in the singlet and triplet (H^- , H) collisions.

A comparison of the scattering (or electron-transfer) and electron-detachment cross sections for the various sets of complex potentials shown in Fig. 2 is given in Table I.

F. Isotope Effects

In this section, the isotope effects in the collisional processes are investigated. The basic effects resulting from the replacement of hydrogen by its isotopes in the (H^- , H) collision system are kinematical.^{9,31,32}

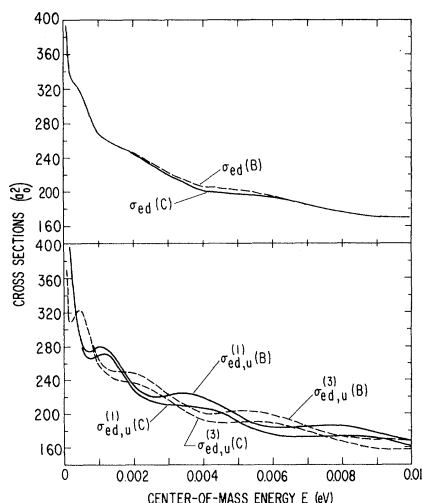


FIG. 29. Comparison of the electron-detachment cross section [Eq. (4.37)] and its constituent *gerade* and *ungerade* contributions [Eqs. (4.40)–(4.43)] as functions of energy in (H^- , H) collisions as predicted by the sets B and C of complex potentials (see Fig. 2) in the c. m. system.

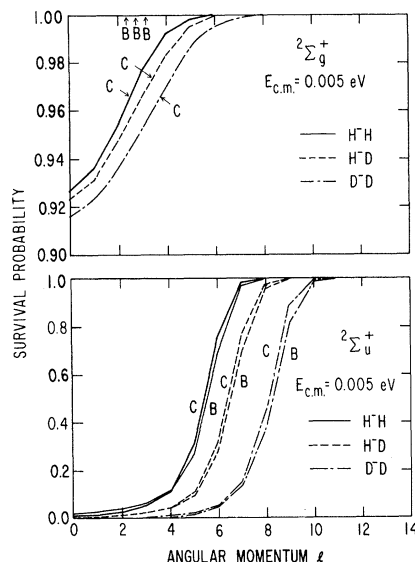


FIG. 30. Comparison of isotope effects in the electron survival-probability $p_l^{(g,u)}$ [Eq. (4.4)] as a function of the angular momentum l at a c. m. energy of 0.005 eV as predicted by the sets B and C of complex potentials (see Fig. 2).

The change in the zero-point energies from the ${}^2\Sigma_u^+H_2^-$ and the ${}^1\Sigma_g^+H_2$ potential wells due to isotope substituting does not give rise to significant effects in scattering, electron-transfer, and collisional-detachment processes. Its effect on associative detachment (or dissociative attachment) would be significant if the detailed partial cross sections⁶ are examined. In this work, we investigate the detachment cross sections as a whole without detailed analysis of the final states of the products. The isotope effect due to the zero-point energy is not expected to be observed.

A large isotope effect comes from the mass dependence of the imaginary parts of the phase shift which appear in the cross section as the survival probabilities (see Sec. IV. A). In Figs. 30 and 31 the isotope effect in survival probability is shown as a function of angular momentum l for c. m. energies 0.005 and 0.5 eV. It is seen that the survival probability as expected decreases with increasing mass.^{28,31} The amount of change predicted by set-B and set-C potentials is in reasonable agreement.

A comparison of the isotope effects in the differential cross section is given in Figs. 32–34 for the theoretical and semiempirical sets of complex potentials. It is seen that in general the cross sections are enhanced by the isotope substitutions. In the case of (H^- , D) [or (D^- , H)] collisions, the isotope substitution also removes the nuclear symmetry, so that Eq. (4.15) no longer holds. From Fig. 34, it is seen that the oscillations due to the

TABLE I. Cross section (a_0^2) for (H⁻, H).

c. m. energy	Set ^a	σ_g^b	σ_u^b	σ_s^c	$\sigma_{ed}^{(g)d}$	$\sigma_{ed}^{(u)e}$	σ_{ed}^f
0.005 eV	B	628.60	155.20	783.76	0.00	201.62	201.62
	C	135.48	145.68	281.16	6.92	190.28	197.20
	D	135.48	139.12	274.60	6.92	186.06	192.96
	E	199.16	54.92	254.08	6.72	76.94	83.66
	F	204.20	45.28	249.52	0.40	70.90	71.30
	G ^g	204.56	72.52	277.08	0	0	0
0.05 eV	B	519.04	137.88	656.92	0.00	108.16	108.16
	C	93.84	143.12	237.00	21.74	99.38	121.12
	D	93.84	131.52	225.36	21.74	105.10	126.84
	E	137.00	41.72	180.76	38.08	45.14	83.20
	F	170.04	37.60	207.64	4.44	45.74	50.18
	G ^g	174.32	110.96	285.28	0	0	0
0.5 eV	B	374.24	149.72	523.96	19.92	27.02	46.96
	C	53.84	124.08	177.92	32.68	39.24	70.96
	D	53.84	122.68	176.52	32.68	43.44	76.12
	E	70.48	44.48	115.00	58.30	20.62	78.90
	F	108.12	29.80	137.92	25.28	31.98	57.26
	G ^g	134.04	63.96	198.00	0	0	0

^aThe potentials labeled B-F are given in Fig. 2.^bSee Eq. (4.32).^cSee Eq. (4.31).^dSee Eq. (4.38).^eSee Eq. (4.39).^fSee Eq. (4.37).^gThis potential is obtained from set E (or F) with the imaginary parts omitted.

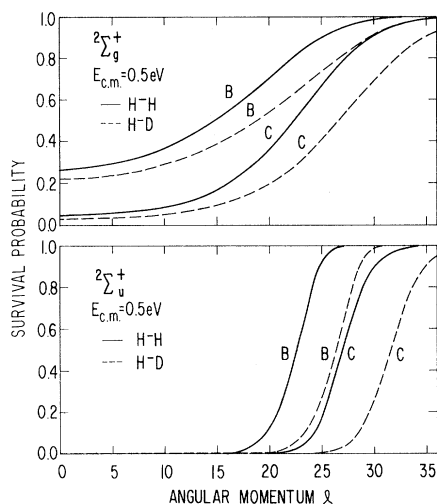


FIG. 31. Comparison of isotope effects in the electron-survival probability $p_l(g, u)$ [Eq. (4.4)] as a function of the angular momentum at a c.m. of 0.5 eV as predicted by the sets B and C of complex potentials (see Fig. 2).

interference between the *gerade* and *ungerade* modes of interactions now become, in the absence of nuclear symmetry interference, regular at large scattering angles. For the same reason, the small oscillation in the differential detachment cross section at large angles are also removed. The oscillations at small angles which come, as mentioned before, from the diffraction scattering, are not affected by the removal of nuclear symmetry.

To investigate the multipath interference and the rainbow-scattering effects without the complication of nuclear-symmetry interference, we have plotted in Fig. 35 the *gerade*, *ungerade*, and their interference contributions to the (H^- , D) collisions for set-C potentials under two circumstances – one with and the other without the imaginary parts

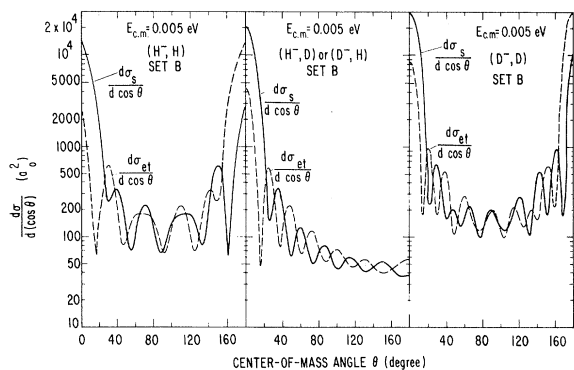


FIG. 32. Isotope effects in the differential scattering and electron-transfer cross sections [Eq. (4.14)] as predicted by complex potential B (see Fig. 2) at an energy of 0.005 eV in the c.m. system.

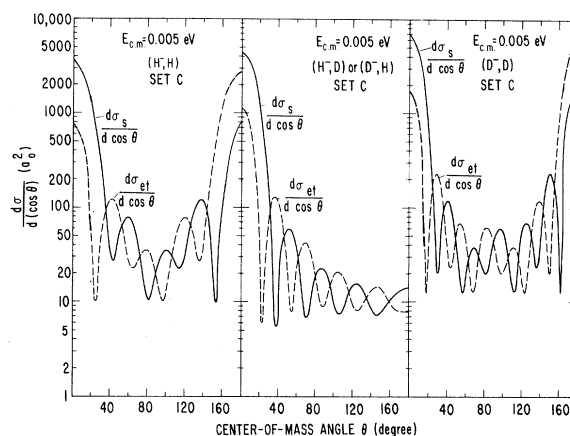


FIG. 33. Isotope effects in the differential scattering and electron-transfer cross sections [Eq. (4.14)] as predicted by complex potential C (see Fig. 2) at an energy of 0.005 eV in the c.m. system.

of the potentials. The very striking damping effects due to the imaginary parts of the potentials then become evident. From Fig. 35 it is seen that the imaginary potential completely removes the rapid oscillations due to the multipath interference in the *gerade* mode of scatterings. The diffraction interference at small angles remain, however, unchanged.

In Fig. 36 a detailed comparison of the isotope effects in the *gerade* and *ungerade* contributions to the differential electron-detachment cross section is given for set-C potentials. It is seen that the detachment cross section is not significantly affected by the isotope substitution. In this comparison, the detachment cross sections for the (H^- , H) and (D^- , D) systems are averaged over the final-spin orientations as given, for example, by Eqs. (4.22) and (4.23) for the (H^- , H) system. The nuclear-symmetry interference is seen to appear for the (H^- , H) and (D^- , D) systems in both the *gerade* and the *ungerade* contributions to the detachment cross section. When the nuclear symmetry is removed as in the (H^- , D) system, the interference structures disappear in both the *gerade* and *ungerade* contributions.

Comparisons of isotope effects in the electron-detachment and electron-transfer probabilities are given in Figs. 37 and 38. It is seen that the probabilities are not appreciably affected by the enhancement in the differential cross sections resulting from the isotope substitution.

The isotope effects of the scattering (or electron-transfer) and electron-detachment cross sections are given in Table II.

ACKNOWLEDGMENT

We are grateful to Dr. Jerry L. Peacher for his helpful discussions.

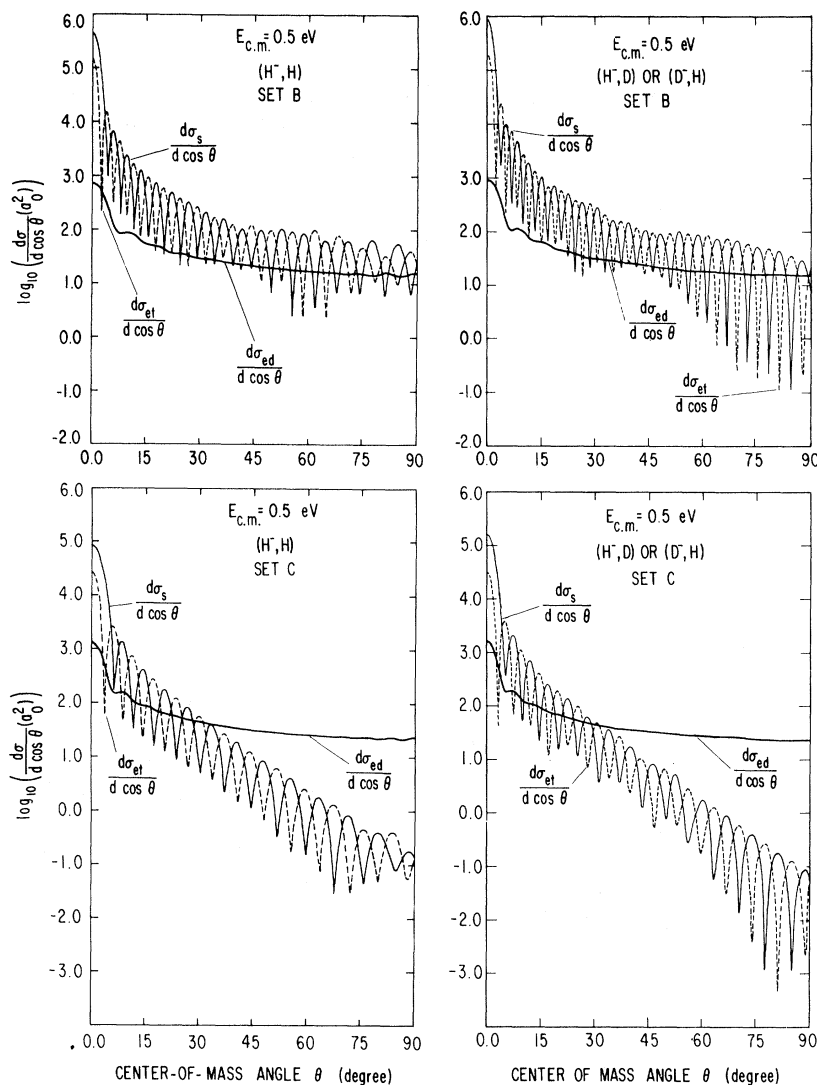


FIG. 34. Comparison of isotope effects in the differential scattering, electron-transfer, and electron-detachment cross sections [Eqs. (4.14) and (4.21)] as predicted by the sets B and C of complex potentials at an energy of 0.5 eV in the c.m. system.

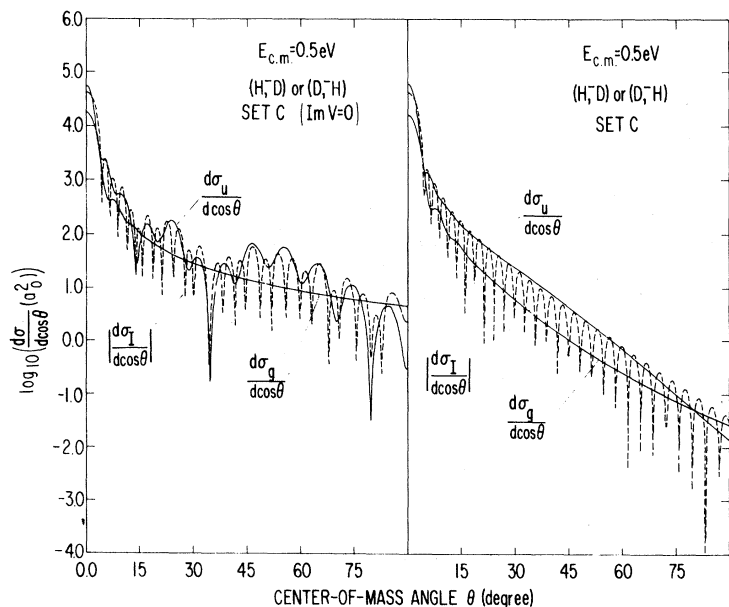


FIG. 35. The damping of the multipath interference in the differential cross section for the (H⁻, D) collision system as predicted by set-C potentials.

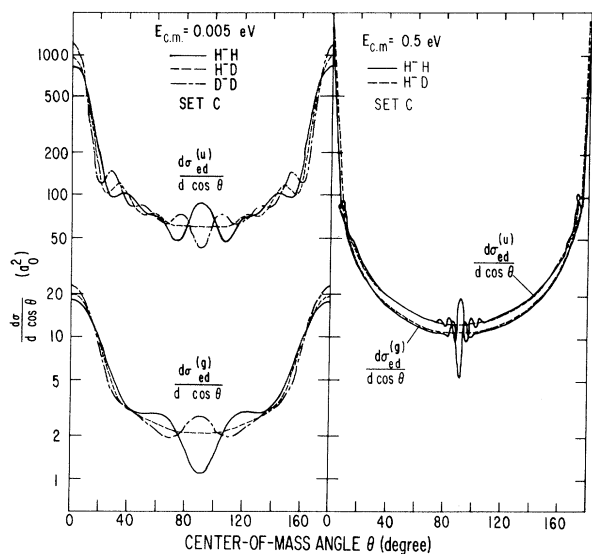


FIG. 36. Comparison of isotope effects in the *gerade* and *ungerade* contributions to the differential electron-detachment cross sections as predicted by complex potential C (see Fig. 2) at energies 0.005 and 0.5 eV in the c.m. system.

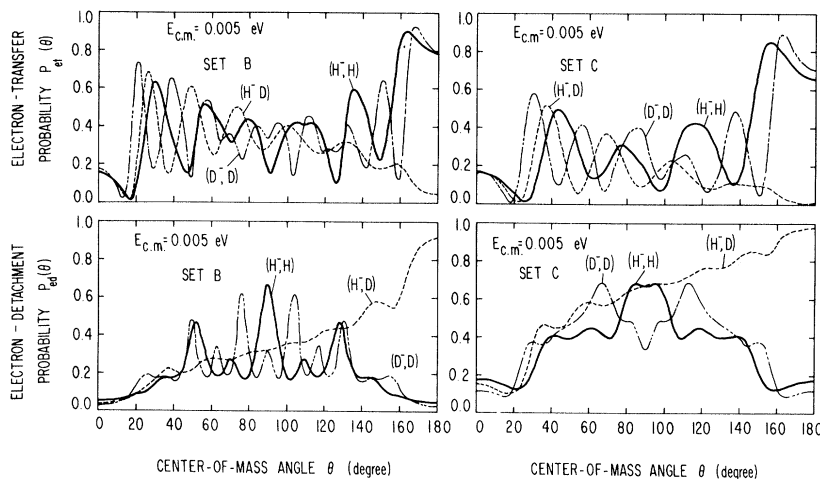


FIG. 37. Comparison of the isotope effects of the electron-transfer and electron-detachment probabilities [Eqs. (4.25) and (4.26)] as predicted by the sets B and C of complex potentials (see Fig. 2) at a c.m. energy of 0.005 eV.

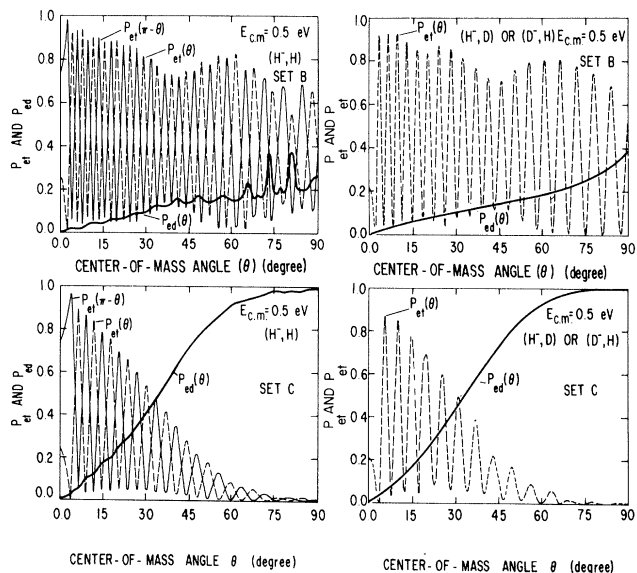


FIG. 38. Comparison of the isotope effects on the electron-transfer and electron-detachment probabilities [Eqs. (4.25) and (4.26)] as predicted by the sets B and C of complex potentials (see Fig. 2) at a c.m. energy of 0.5 eV.

TABLE II. Cross section (a_0^2).

c. m. energy	System	Set B ^a			Set C ^a		
		σ_b	σ_{et}^b	σ_s^b	σ_{ed}^c	σ_{et}^b	σ_{ed}^c
0.005 eV	H ⁻ H	783.76	783.76	281.16	201.62	281.16	197.20
	H ⁻ D	598.41	237.99	222.13	199.31	72.74	196.98
	D ⁻ D	890.08	890.08	312.12	198.54	312.12	195.22
0.05 eV	H ⁻ H	656.92	656.92	237.00	108.16	237.00	121.12
	H ⁻ D	474.28	216.91	178.41	107.81	62.33	122.38
0.5 eV	H ⁻ H	523.96	523.96	177.92	46.96	177.92	71.92
	H ⁻ D	363.75	182.65	136.81	48.45	49.87	73.97

^aSet-B and set-C potentials are given in Fig. 2.

^bCalculated according to Eq. (4.31) with appropriate averaging over the nuclear-spin multiplicities such as, for example, given by Eq. (4.32) for the (H⁻, H) system.
^cCalculated according to Eq. (4.37) with appropriate averaging over the nuclear-spin multiplicities such as, for example, given by Eqs. (4.38) and (4.39) for the (H⁻, H) system.

*Research supported by the Advanced Research Projects Agency of the Department of Defense and monitored by the U. S. Army Research Office, Durham under Contract DA-31-124-ARO-D-257.

¹J. C. Y. Chen, Phys. Rev. **156**, 12 (1967).

²A. Herzenberg, Phys. Rev. **160**, 80 (1967).

³J. N. Bardsley, Proc. Roy. Soc. (London) **91**, 300 (1967).

⁴A. Dalgarno and J. C. Browne, Astrophys. J. **149**, L231 (1967).

⁵A. L. Schmeltekopf, F. C. Fehsenfeld, and E. E. Ferguson, Astrophys. J. **148**, L155 (1967).

⁶J. C. Y. Chen and J. L. Peacher, Phys. Rev. **168**, 56 (1968).

⁷A. L. Fetter and K. M. Watson, in *Advances in Theoretical Physics*, edited by K. A. Brueckner (Academic Press Inc., New York, 1965), p. 115-194.

⁸J. N. Bardsley, A. Herzenberg, and F. Mandl, Proc. Roy. Soc. (London) **89**, 305 (1966).

⁹J. C. Y. Chen and J. L. Peacher, Phys. Rev. **167**, 30 (1968).

¹⁰I. Eliezer, H. S. Taylor, and J. K. Williams, J. Chem. Phys. **42**, 2165 (1967).

¹¹A brief account of this work was presented at the American Physical Society Winter Meeting at San Diego, Bull. Am. Phys. Soc. **13**, 1655 (1968).

¹²M. L. Goldberger and K. M. Watson, *Collision Theory* (John Wiley & Sons, Inc., New York, 1964).

¹³For a recent review, see K. M. Watson, in *Atomic Physics*, edited by B. Bederson, V. W. Cohen, and F. M. J. Pichanick (Plenum Press, New York, 1969), p. 333-352.

¹⁴H. Feshbach, Ann. Phys. (N. Y.) **19**, 287 (1962).

¹⁵J. C. Y. Chen, Phys. Rev. **152**, 1454 (1966).

¹⁶Such a channel projector for electron-detachment channels has not been constructed in a closed form. The expression obtained in Ref. 1 for associative-detachment channels cannot be adopted in the coupled-channel equations [Eq. (2.13)] in a straightforward manner.

¹⁷For details, see J. C. Y. Chen, in *Advances in Radiation Chemistry*, edited by M. Burton and J. L. Magee (John Wiley & Sons, Inc., New York, 1968), Vol. I.

¹⁸J. C. Y. Chen, in *Proceedings of the Fifth International Conference on the Physics of Electronic and Atomic Collisions* (Publishing House, Nauka, Leningrad, USSR, 1967), p. 332.

¹⁹A. Herzenberg and F. Mandl, Proc. Roy. Soc. (London) **A274**, 253 (1963).

²⁰D. Rapp, T. E. Sharp, and D. D. Briglia, Phys. Rev. Letters **14**, 533 (1965) (for dissociative attachment via the *gerade* mode of interaction).

²¹G. J. Schulz and R. K. Asundi, Phys. Rev. **158**, 25 (1967) (for dissociative attachment via the *ungerade* mode of interaction).

²²G. J. Schulz, Phys. Rev. **135**, A988 (1964).

²³H. Ehrhardt, L. Langhans, F. Linder, and H. S. Taylor, Phys. Rev. **173**, 222 (1968).

²⁴J. N. Bardsley, A. Herzenberg, and F. Mandl, Proc. Roy. Soc. (London) **89**, 321 (1966).

²⁵D. G. Hummer, R. F. Stebbings, W. L. Fite, and

L. M. Branscomb, *Phys. Rev.* **119**, 668 (1960).

²⁶T. Holstein, *Phys. Rev.* **84**, 1073 (1951). Similar concepts have been suggested by Bates [*Phys. Rev.* **78**, 492 (1950)] for the process of dissociative recombination.

²⁷J. N. Bardsley, A. Herzenberg, and F. Mandl, in *Atomic Collision Processes*, edited by M. R. C. McDowell (North-Holland Publishing Co., Amsterdam, 1964), p. 415.

²⁸J. C. Y. Chen and J. L. Peacher, *Phys. Rev.* **163**, 103 (1967). We take this occasion to point out that in the caption of Figs. 2 and 3 and in Tables I, II, and IV of this reference, "L" should read "J".

²⁹For low energies, it is not a trivial question whether one can distinguish by experiment between electron-transfer collisions and scattering for a symmetrical system such as (H^- , H). Theoretically, the same definition of (and expressions for) differential cross sections for electron transfer and scattering may be adopted for both the high-energy and low-energy collisions.

³⁰J. C. Y. Chen and J. L. Peacher, in *Proceedings of the Conference on Heavy Particle Collisions* (Queen's University of Belfast, N. Ireland, 1968), Abstract.

³¹Yu. N. Demkov, *Phys. Letters* **15**, 235 (1965).

³²T. F. O'Malley, *Phys. Rev.* **150**, 14 (1966).

Application of the Pseudopotential Method to Atomic Scattering

J. Callaway and P. S. Laghos

Department of Physics, Louisiana State University, Baton Rouge, Louisiana 70803

(Received 8 May 1969)

The empirical pseudopotential method is discussed and applied to a calculation of the spin-exchange cross section in collisions of Na and Cs atoms. The difference between potential energy curves for the lowest singlet and triplet states of the Na-Cs system is calculated by the Heitler-London method, using a Hamiltonian in which the effects of tightly bound electrons are replaced by a pseudopotential. Wave functions for the free atoms are found by numerical integration using the pseudopotential, and agree well with the exact valence-electron functions at large distances. The scattering phase shifts are calculated in the WKB approximation, and the cross section computed from them is averaged over a Boltzmann distribution of relative velocities. At a temperature of 500°K, the averaged reduced spin-exchange cross section is 1.5×10^{-14} cm².

I. INTRODUCTION

Knowledge of interatomic forces is of great importance for many problems in astronomy, physics, and chemistry. If the interacting atoms contain only a few electrons, reasonably accurate calculations from first principles are possible. In the case of heavy atoms, some simplifications must be introduced. The objective of the present work is to apply the pseudopotential method, which has been extensively used in solid-state physics to the calculation of the interactions of heavy atoms. Substantial simplifications result. The method is then applied to the interaction of Na and Cs atoms, and, in particular, to the calculation of the spin-exchange cross section.

The general concept of the pseudopotential method can be explained qualitatively with reference to an example; to be specific, consider Na. Frequently, one thinks of Na as an one electron atom even though it contains 11 electrons. The idea of

an one-electron system is reasonably legitimate, since under usual circumstances the electrons in the closed 1s, 2s, and 2p shells are inert. However, their presence greatly complicates calculations, because the wave function of the active, 3s electron must be orthogonal to the wave functions of electrons in closed shells, and consequently must vary rapidly near a nucleus. It becomes necessary to include core wave functions in many calculations in which only the valence electrons are of real interest. In the atomic interaction problem, one must include the interaction between the valence electrons on one atom and the core electrons on the other. It is greatly desirable to simplify such calculations by removing the core electrons from the problem. This is accomplished by the pseudopotential.

To see how this is possible, we note that the effect of the core electrons on the valence electron is repulsive. In Na, the energy of the lowest state of the valence electron is -0.378 Ry,